

# Migration of small moons in Saturn's rings

Benjamin C. Bromley

*Department of Physics & Astronomy, University of Utah,  
115 S 1400 E, Rm 201, Salt Lake City, UT 84112*

bromley@physics.utah.edu

Scott J. Kenyon

*Smithsonian Astrophysical Observatory,  
60 Garden St., Cambridge, MA 02138*

skenyon@cfa.harvard.edu

## ABSTRACT

The motions of small moons through Saturn's rings provide excellent tests of radial migration models. In theory, torque exchange between these moons and ring particles leads to radial drift. We predict that moons with Hill radii  $r_H \sim 2\text{--}24$  km should migrate through the A ring in 1000 yr. In this size range, moons orbiting in an empty gap or in a full ring eventually migrate at the same rate. Smaller moons or moonlets – such as the propellers (e.g., Tiscareno et al. 2006) – are trapped by diffusion of disk material into corotating orbits, creating inertial drag. Larger moons – such as Pan or Atlas – do not migrate because of their own inertia. Fast migration of 2–24 km moons should eliminate intermediate-size bodies from the A ring and may be responsible for the observed large-radius cutoff of  $r_H \sim 1\text{--}2$  km in the size distribution of the A ring's propeller moonlets. Although the presence of Daphnis ( $r_H \approx 5$  km) inside the Keeler gap challenges this scenario, numerical simulations demonstrate that orbital resonances and stirring by distant, larger moons (e.g., Mimas) may be important factors. For Daphnis, stirring by distant moons seems the most promising mechanism to halt fast migration. Alternatively, Daphnis may be a recent addition to the ring that is settling into a low inclination orbit in  $\sim 10^3$  yr prior to a phase of rapid migration. We provide predictions of observational constraints required to discriminate among possible scenarios for Daphnis.

*Subject headings:* planetary systems – solar system: formation

## 1. Introduction

Migration is the steady radial drift of a massive planet or satellite through an astrophysical disk (e.g., Lin & Papaloizou 1986; Ward 1997; Artymowicz 2004; Levison et al. 2007; Papaloizou et al. 2007; Kirsh et al. 2009; D'Angelo et al. 2010; Lubow & Ida 2010, and references therein). When a

planet lies embedded in a disk of gas or solid particles, it tries to clear material from its orbit. Clearing by a massive planet creates wakes inside and outside its orbit. These density perturbations exert a torque on the planet, which produces an inwards or outwards migration through the disk. Analytic and numerical calculations show that, in many cases, isolated planets migrate through the disk on a timescale much shorter than the disk lifetime (Goldreich & Tremaine 1979; Lin & Papaloizou 1979; Goldreich & Tremaine 1980; Ida et al. 2000; Tanaka et al. 2002; Papaloizou et al. 2007; Kirsh et al. 2009).

This process provides a popular explanation for the architectures of many planetary systems. Migration plausibly accounts for the orbits of some “hot Jupiters” very close to their parent stars (e.g., Masset & Papaloizou 2003; Alexander & Armitage 2009, and references therein) and the compact orbital configurations of several multiplanet systems, including Kepler 11 which has five super-Earths orbiting within 0.3 AU of a Sun-like star (Lissauer et al. 2011). In our own solar system, migration appears to be a key dynamical mechanism for arranging the orbits of the outer planets (Malhotra 1993; Hahn & Malhotra 1999; Levison et al. 2007; Morbidelli et al. 2007).

Despite its broad applicability in exoplanetary systems, testing the predictions of migration theory is challenging. In a young planetary system, growing protoplanets gravitationally stir particles in the disk and limit the formation of coherent density wakes (Bromley & Kenyon 2011b). For a single planet, migration through a gaseous disk also depends on the dynamical and thermal state of the disk (e.g., Paardekooper et al. 2010, 2011). Real disks contain several planets in a constantly evolving mix of gas and solid particles (e.g., Bromley & Kenyon 2011a; Youdin & Kenyon 2012, and references therein). Current calculations only partially address this complexity (e.g., Masset & Snellgrove 2001; Morbidelli et al. 2007; D’Angelo & Marzari 2012). Thus, theory is hard-pressed to derive robust predictions applicable to observed systems.

Saturn’s rings provide an interesting laboratory in which to test migration theory. The A ring is a geometrically thin disk of solid particles with orbital periods shorter than a terrestrial day. Aside from countless cm- to m-sized particles (e.g., Cuzzi et al. 2009), the rings contain many 0.1 to 1 km moonlets that could easily migrate through the disk (Tiscareno et al. 2010). NASA’s Cassini-Huygens missions have also revealed a variety of density perturbations within the rings (Colwell et al. 2009), identified a herd of “propeller” moonlets (named for the wakes of ring particles they create; Tiscareno et al. 2006, 2008), and discovered the small moons Pan and Daphnis (Showalter 1991; Porco et al. 2005). Together, these features allow robust tests of our understanding of gravity and dynamics in a complicated system of solid particles (see also Cuzzi et al. 2010; Esposito 2010, and references therein).

Previous theoretical analyses of migration in Saturn’s rings have concentrated on the non-Keplerian, radial motion of propeller moonlets within the A ring (Tiscareno et al. 2010). These motions may result from interactions between moonlets and stochastic density fluctuations in the disk (Crida et al. 2010; Rein & Papaloizou 2010; Pan et al. 2012) or between moonlets and ring particles on loosely bound “frog” orbits around the moonlet (Pan & Chiang 2010, 2012). These phenomena, or perhaps direct collisions between moonlets and large ring particles, may *cause* the observed radial motion in some moonlets. On the other hand, large-scale ring structure, particularly radial density waves, may provide torques that *suppress* radial motion (Tiscareno 2012). In this

picture, the observed non-Keplerian orbits come from recent kicks received by moonlets, which then settle back to their original Keplerian configuration. Fortunately, each of these theoretical scenarios makes a unique prediction for the evolution of moonlet orbits. Upcoming Cassini observations will be able to distinguish among them (Tiscareno 2012).

Here, we focus on other modes of migration for moonlets and small moons embedded in Saturn’s 17,000 km wide A ring<sup>1</sup>. Aside from stochastic interactions, larger moonlets and small moons like Daphnis are candidates for “fast” migration modes that satellites experience in a dynamically cold, planetesimal disk (Ida et al. 2000). Because fast migration is a critical component of migration theory in exoplanetary systems, understanding fast modes in Saturn’s rings improves our ability to predict migration in a broad range of environments.

We begin with a theoretical overview of migration in a particle disk (§2) and then specialize the theoretical estimates to conditions appropriate for Saturn’s A ring (§3). In §4, we confirm the analytic estimates with numerical simulations, but demonstrate that stochastic effects, resonances with more distant moons, and stirring by distant moons can slow down or halt migration of small satellites through the ring. In §5, we examine the migration of Daphnis, which is located within the Keeler gap. If Daphnis only interacts with ring particles, its migration should be fast and detectable with current satellites. However, orbital resonances (e.g., Prometheus 32:31) and stirring by moons out of the ring plane (e.g., Mimas and Tethys) may have a strong impact on Daphnis’ orbit and migration rate. Measuring the evolution of Daphnis’ orbit can constrain these possibilities. We conclude in §6 with a brief summary.

## 2. Migration in a particle disk

To test migration theory in Saturn’s rings, we develop basic predictions for an idealized disk of solid particles orbiting a much more massive planet. For any satellite within the disk, the Hill radius,  $r_H$ , defines a spherical surface where the gravity of the satellite roughly balances the gravity of the planet. This radius also characterizes the annular width of the satellite’s corotation zone, an annulus where disk particles on nearly circular orbits oscillate back and forth in the satellite’s rotating reference frame (e.g., on horseshoe orbits). Here we take the halfwidth of the corotation zone to be  $X_{co}r_H$ , with  $X_{co} = 2$  (e.g., Bromley & Kenyon 2011b). When the corotation zone is full of small particles, migration is not efficient.

Two physical processes set the density of smaller particles in the corotation zone. The massive satellite gravitationally scatters smaller particles out of the zone. Viscous spreading drives the diffusion of smaller particles back into the zone. When scattering overcomes diffusion, the satellite opens up a physical gap in the disk. For convenience, we define  $r_{\text{gap}}$  as the Hill radius of the smallest satellite capable of clearing out its corotation zone (see also Lissauer et al. 1981; Rafikov 2001). When the corotation zone is nearly clear of smaller particles, migration can be very efficient.

---

<sup>1</sup>In the spirit of the definitions in Tiscareno (2013), we use “moonlet” to describe any of a numerous and perhaps unresolved population with physical radii of  $\lesssim 1$  km and “small moon” to refer to the larger objects Daphnis, Pan or Atlas.

When a satellite has  $r_{\text{H}} > r_{\text{gap}}$ , it undergoes fast migration. In this situation, the satellite can gravitationally pull corotating material *all the way past* its corotation zone, hauling itself radially inward or outward like a rope climber. In gaseous disks, this mode of migration is often called ‘type III’ (Masset & Papaloizou 2003) to distinguish it from the slow, type I migration of planets incapable of forming a gap and the intermediate pace of type II migration of more massive planets surrounded by a large gap<sup>2</sup> (Ward 1997; Bryden et al. 1999).

For more massive satellites with  $r_{\text{H}} \gg r_{\text{gap}}$ , fast migration stalls. As the mass of a satellite grows, its Hill radius – and the width of its corotation zone – also grows. At some point, the satellite cannot scatter particles out of the corotation zone fast enough: some disk material remains inside the corotation zone and interacts with the planet. This interaction reduces the torque and slows migration. We define  $r_{\text{fast}}$  as the Hill radius where fast migration begins to stall. Thus, satellites with  $r_{\text{gap}} < r_{\text{H}} < r_{\text{fast}}$  undergo fast migration.

In physical units, the three critical Hill radii for fast migration are:

$$r_{\text{H}} \equiv a \left( \frac{m}{3M} \right)^{1/3}, \quad [\text{Hill radius}], \quad (1)$$

$$r_{\text{gap}} \approx 0.4 (\nu_{\text{rad}} a T)^{1/3}, \quad [\text{minimum } r_{\text{H}} \text{ to form a gap}], \quad (2)$$

$$r_{\text{fast}} = 1.7 a \left( \frac{a^2 \Sigma}{M} \right)^{1/2} \quad [\text{maximum } r_{\text{H}} \text{ for fast migration}]. \quad (3)$$

In these expressions,  $m$  is the mass of an object orbiting with semimajor axis  $a$  and period  $T$  around a central star or planet with mass  $M$ . The disk has surface density  $\Sigma$  and radial viscosity  $\nu_{\text{rad}}$ .

Deriving  $r_{\text{gap}}$  and  $r_{\text{fast}}$  relies on identifying important timescales in the disk. Rates of migration are set by the satellite’s Keplerian orbital period  $T$ . Although an oblate planet and gravitational perturbations by surrounding massive moons prevent a satellite from executing standard Keplerian orbits, the Keplerian orbital period is a useful fiducial for all other timescales. Close encounters between the satellite and particles occur every synodic period  $T_{\text{syn}}$ , the timescale for particles on orbits with separation  $\Delta a$  to return to the same orbital phase. Massive satellites scatter particles away from their orbits, opening a gap of half-width  $\Delta a$  within the disk clearing time,  $T_{\text{clear}}$ . For particle disks, the disk clearing time for a small gap is a few times larger than  $T_{\text{syn}}$  (e.g., Kirsh et al. 2009). Viscous processes between disk particles fill gaps on the viscous (or gap-filling) time  $T_{\text{fill}}$ , which depends on the disk’s radial viscosity  $\nu_{\text{rad}}$  (e.g., Lissauer et al. 1981; Hourigan & Ward 1984).

Physical collisions damp the velocities of disk particles on the damping timescale  $T_{\text{damp}}$ . Collisional damping is a random walk-type process that depends on  $\lambda_{\text{rad}}$ , the radial distance between collisions, and  $f_{\text{loss}}$ , the fractional loss of kinetic energy per particle in a collision (equivalent to the square of the coefficient of restitution). The mean-free-path  $\lambda$  is related to the optical depth  $\tau$  (e.g., Cook & Franklin 1964; Goldreich & Tremaine 1978a). In the low optical depth limit, a ring

---

<sup>2</sup> In a gaseous disk, uncertainties in the disk viscosity (and hence the radial and vertical gradients in the pressure, temperature, and other physical variables) make migration calculations very challenging. Thus, it is uncertain whether type III migration is possible in a gaseous disk. In a particle disk, though, Type III migration is generally accepted. Starting with Malhotra (1993) and continuing with Ida et al. (2000), Kirsh et al. (2009), and Bromley & Kenyon (2011b), fast/rapid/runaway migration is a standard phenomenon in particle disks.

of monodisperse particles with radius  $r_p$  has  $\tau = 3\Sigma/4\rho_p r_p$ , where  $\rho_p$  is the particle mass density (Goldreich & Tremaine 1978a; Salmon et al. 2010). A more general, realistic treatment of optical depth requires consideration of the particle size distribution and coherent structures that may form as a result of self-gravity (e.g., Salo & Karjalainen 2003; Tiscareno 2013).

For  $\Delta a \ll a$ , these timescales are:

$$T \equiv 2\pi \left( \frac{a^3}{GM} \right)^{1/2} \quad [\text{orbital period}], \quad (4)$$

$$T_{\text{syn}} \approx \frac{2aT}{3\Delta a} \quad [\text{synodic period for orbital separation } \Delta a], \quad (5)$$

$$T_{\text{clear}} \approx 4T_{\text{syn}} \quad [\text{gap clearing time (half-width } \Delta a)], \quad (6)$$

$$T_{\text{fill}} \approx \frac{(2\Delta a)^2}{\nu_{\text{rad}}} \quad [\text{gap filling/viscous diffusion}], \quad (7)$$

$$T_{\text{damp}} \approx \frac{\lambda_{\text{rad}}^2}{f_{\text{loss}} \nu_{\text{rad}}} \approx \frac{4r_p \rho_p a}{3f_{\text{loss}} v_{\text{Kep}} \Sigma} \quad [\text{damping time}]. \quad (8)$$

To derive the physical scales for fast migration, we compare the timescales for the relevant processes. When  $T_{\text{clear}} = T_{\text{fill}}$ , a satellite clears its corotation zone as fast as viscous spreading fills the zone back up. This equality defines  $r_{\text{gap}}$ , the smallest Hill radius for a satellite capable of opening a gap in the disk. Balancing the torque from the satellite on disk material with the torque from the disk on the satellite is roughly equivalent to setting  $T_{\text{clear}} = T_{\text{fill}}$  and yields similar expressions for  $r_{\text{gap}}$  (e.g., Lissauer et al. 1981; Hourigan & Ward 1984; Ward & Hourigan 1989; Ward 1997; Rafikov 2001).

Aside from establishing which satellites can open gaps in the disk,  $r_{\text{gap}}$  sets a lower limit on the Hill radii of satellites capable of undergoing fast migration (Ida et al. 2000; Masset & Papaloizou 2003; Kirsh et al. 2009; Bromley & Kenyon 2011b). When a satellite pulls disk material near the edge of its corotation zone across its orbit, it recoils in the opposite direction. If the net recoil is large enough, the satellite does not interact with scattered particles when they pass by the satellite one synodic period later. Satellites with  $r_{\text{H}} < r_{\text{gap}}$  cannot clear their corotation zones and do not recoil enough to overcome the inertia of material along their orbits. Satellites with  $r_{\text{H}} \gg r_{\text{gap}}$  do not recoil enough to avoid a second encounter with scattered particles.

To determine the range of Hill radii for satellites that undergo fast migration, we identify the maximum Hill radius where the time for a satellite to move a radial distance equal to the width of its corotation zone is less than the synodic period of particles at the edge of the corotation zone (see also Ida et al. 2000; Masset & Papaloizou 2003; Kirsh et al. 2009; Bromley & Kenyon 2011b). To derive this Hill radius, which we define as  $r_{\text{fast}}$ , we set  $T_{\text{syn}} = \eta r_{\text{fast}} [da_{\text{fast}}/dt]^{-1}$  where  $da_{\text{fast}}/dt$  is the fast migration rate<sup>3</sup> (e.g., eq. 12 below; see also Ida et al. 2000). To avoid repeat encounters with material on horseshoe orbits within the corotation zone, we set  $\eta = 2$ . Although choosing  $\eta = 3.5$  would eliminate all possible repeat encounters, material trapped on horseshoe orbits provides most of the drag on a drifting moonlet. Thus, we choose  $\eta = 2$ .

For disks of solid particles, the viscosity  $\nu_{\text{rad}}$  depends on kinematics. <sup>3</sup>From Goldreich & Tremaine

---

<sup>3</sup>Bromley & Kenyon (2011a) derive this rate from the recoil due to a single scattering event and an encounter frequency integrated over the width of the corotation zone.

(1978a, and references therein), the viscosity is a function of the optical depth, the orbital period, and the radial velocity dispersion of particles  $v_p$ :

$$\nu_{\text{rad}} \approx \frac{v_p^2 T}{4\pi} \frac{\tau}{1 + \tau^2} . \quad (9)$$

When  $\tau$  is small,  $\nu_{\text{rad}} \propto \tau$ ; when  $\tau$  is large,  $\nu_{\text{rad}} \propto \tau^{-1}$ .

In addition to the surface density and the viscosity, the vertical scale height of the disk  $h$  also plays an important role in satellite migration (e.g., Lin & Papaloizou 1979; Goldreich & Tremaine 1980; Ward 1997; Ida et al. 2000; Papaloizou et al. 2007; Bromley & Kenyon 2011b). For a disk of particles, the scale height depends on the vertical velocity dispersion  $v_z$ :

$$h = v_z \Omega^{-1} , \quad (10)$$

where  $\Omega$  is the local angular velocity of particles. If disk particles follow a Rayleigh distribution,  $v_z \approx v_p/2$  (e.g., Ohtsuki 1992, and references therein). The local (3-D) viscosity then scales approximately as  $\nu \propto h^2$  as in the  $\alpha$  prescription for turbulent gaseous disks (Shakura & Sunyaev 1973; Pringle 1981). The true relationship between  $v_z$  and the mean 3-D velocity dispersion is more complicated, especially in Saturn’s A ring where self-gravity wakes can increase velocities in the plane of the ring (Tiscareno et al. 2007).

With these definitions and physical expressions for critical parameters, the theoretical radial drift rates for the three modes of migration are:

$$\frac{da_{\text{emb}}}{dt} \approx -64 \frac{\pi a^2 \Sigma}{M} \frac{r_{\text{H}}^3}{h^2 a} \frac{a}{T} \quad r_{\text{H}} \lesssim h, r_{\text{gap}} \quad [\text{embedded, no gap; Type I}] \quad (11)$$

$$\frac{da_{\text{fast}}}{dt} \approx \pm \frac{5.3 \pi a^2 \Sigma}{M} \frac{a}{T} \quad h, r_{\text{gap}} \lesssim r_{\text{H}} \lesssim r_{\text{fast}} \quad [\text{fast; Type III}] \quad (12)$$

$$\frac{da_{\text{gap}}}{dt} \approx -16 \frac{\pi a^2 \Sigma}{M} \frac{r_{\text{H}}}{a} \frac{a}{T} \rightarrow -\frac{3\nu_{\text{rad}}}{2a} \quad r_{\text{H}} \gtrsim r_{\text{gap}} \quad [\text{embedded+gap; Type II}]. \quad (13)$$

When the Hill radius is smaller than the disk scale height and the gap radius, the satellite has a very weak gravity, cannot open up a gap, and produces very weak density perturbations in the disk. Only very slow, embedded migration is possible. Its rate (eq. [11]) follows from weak scattering theory (e.g., Lin & Papaloizou 1979) and is analogous to Type I migration in gaseous disks (Ward 1997). The scale height is important in setting this rate because it is a measure of the distance at which the ring particles transition from random motion to coherent, shear flow from the satellite’s perspective (e.g., Tanaka et al. 2002). Fast migration (eq. [12]) is the ideal case of a satellite spiraling through a dynamically cold disk (Masset & Papaloizou 2003). The rate is independent of satellite mass; the greater gravitational reach of a more massive satellite compensates for its higher inertia. The migration rate for  $r_{\text{H}} > r_{\text{fast}}$  is the Type II analog for a planet which opens a gap in a particle disk (eq. [13]). In the low viscosity limit, differential torques arise from material at the edges of the gap, which lies at or beyond the corotation zone (Bromley & Kenyon 2011b). In the high viscosity limit, the migration rate is set by the viscous timescale (see, e.g., Ward 1997; Papaloizou et al. 2007).

The transition from type I migration with no gap to fast and type II migration with a gap is complex (e.g., Hourigan & Ward 1984; Ward & Hourigan 1989). When a small satellite with  $r_H < r_{\text{gap}}$  accretes disk material and grows to larger radii, it drifts through the disk more rapidly (eq. [11]). If this satellite drifts across its corotation zone more rapidly than it can clear a gap, it drifts through the disk with a partially cleared corotation zone. Because the drift time scales more weakly with mass ( $\propto m^{-1}$ ) than the time to clear a gap ( $\propto m^{-2}$ ), there is a range of satellite masses where a satellite could clear a gap if it could stop drifting (Hourigan & Ward 1984; Ward & Hourigan 1989). This range of masses roughly corresponds to the range where fast migration operates.

The transition from type I to type II migration also depends on the scale height and eccentricity  $e$  of disk particles. When disk particles have large  $e$ , the drift rate slows by a factor  $\sim (r_H/e_p a)^3$  relative to the fast rate (see eq. [12]; Bromley & Kenyon 2011b). When  $h < r_H < r_{\text{gap}}$ , simulations suggest that nonlinearities and other competing effects – such as the inertial drag of material stuck in the corotation zone – substantially reduce the migration in this “transgap” range of Hill radii (D’Angelo et al. 2003). This conclusion is strengthened by a recent analysis of moonlets in the A ring (Tiscareno 2012), which shows how radial density structures in the ring can produce torques that damp radial drift.

For larger satellites with  $r_H \sim r_{\text{fast}}$ , simulations (Bromley & Kenyon 2011b) also suggest that fast migration falls off at least as rapidly as  $(r_{\text{fast}}/r_H)^3$  (see also Syer & Clarke 1995). As  $r_H$  increases ( $r_H > r_{\text{gap}}, r_{\text{fast}}$ ), the satellite can maintain a gap in the disk and can experience migration with a fully-formed gap (eq. [13]). In the inviscid limit of this type II migration (Ward 1997; Crida et al. 2006), the rate is given by weak scattering theory. In a sufficiently viscous disk, material piles up at the gap edges. Then, the timescale for radial drift is the viscous timescale (Bryden et al. 1999).

The sketch in Figure 1 summarizes the various migration modes. In addition to showing the relative magnitude of the rates in equations (11–13) as a function of  $r_H$ , the sketch illustrates the impact of viscosity in the transgap regime and the high- and low-mass fall off of the fast migration mode. Other motions affecting a satellite’s radial drift include stochastic migration (see Rein & Papaloizou 2010; Crida et al. 2010; Pan et al. 2012) and the periodic orbit perturbations caused by material on corotating “frog” orbits centered on the satellite (Pan & Chiang 2010). On yearlong timescales, these drifts (random walks with effective  $da/dt$  values that lie in the shaded region in the figure) can be comparable to linear-in-time radial migration in Saturn’s rings.

### 3. Migration in the A ring

Saturn’s A ring is a dynamically cold, thin disk of icy, meter-sized particles, lying in an annulus around Saturn that extends from a radius of 117,000 km to the Roche Division at 137,000 km. In our calculations, we adopt an orbital radius of  $a = 130,000$  km as representative. For other physical parameters, observations (e.g., Tiscareno et al. 2007; Colwell et al. 2009) suggest:

$$\Sigma = 40 \text{ g/cm}^2 \tag{14}$$

$$h = 10 \text{ m} \tag{15}$$

$$\nu_{\text{rad}} = 85 \text{ cm}^2/\text{s}. \tag{16}$$

Adopting these values allows us to specialize the results of §2 to Saturn’s A ring.

In the A ring, the radii that delineate different modes of migration in equations (1–3) become

$$r_{\text{H}} = 1.7 \left[ \frac{\rho}{1 \text{ g/cm}^3} \right]^{1/3} \left[ \frac{a}{1.3 \times 10^5 \text{ km}} \right] r_{\text{phys}}, \quad (17)$$

$$r_{\text{gap}} \approx 2 \left[ \frac{\nu_{\text{rad}}}{85 \text{ cm}^2/\text{s}} \right]^{1/3} \left[ \frac{a}{1.3 \times 10^5 \text{ km}} \right]^{5/6} \text{ km}, \quad (18)$$

$$r_{\text{fast}} \approx 24 \left[ \frac{a}{1.3 \times 10^5 \text{ km}} \right]^2 \left[ \frac{\Sigma}{40 \text{ g/cm}^2} \right]^{1/2} \text{ km}. \quad (19)$$

With mean densities of  $\sim 0.5\text{--}1 \text{ g/cm}^3$ , the Hill radius and the physical radius of a moonlet or small moon in the A ring are similar. From equation (18), satellites with Hill radii below a few km cannot open a full gap in the A ring. These bodies can only migrate in the slow, embedded mode. Satellites with  $r_{\text{H}} \gtrsim 20 \text{ km}$  are too massive for fast migration. Between a few km and 20 km, small moons can migrate in fast mode.

The timescales in equations (4–8) specialize to

$$T \approx 0.0015 \left[ \frac{a}{1.3 \times 10^5 \text{ km}} \right]^{3/2} \text{ yr}, \quad (20)$$

$$T_{\text{syn}} \approx 130 \left[ \frac{1 \text{ km}}{\Delta a} \right] \left[ \frac{a}{1.3 \times 10^5 \text{ km}} \right]^{5/2} \text{ yr}, \quad (21)$$

$$T_{\text{clear}} \approx 520 \left[ \frac{1 \text{ km}}{\Delta a} \right] \left[ \frac{a}{1.3 \times 10^5 \text{ km}} \right]^{5/2} \text{ yr}, \quad (22)$$

$$T_{\text{fill}} \approx 3.7 \left[ \frac{\Delta a}{1 \text{ km}} \right]^2 \left[ \frac{85 \text{ cm}^2/\text{s}}{\nu_{\text{rad}}} \right] \text{ yr}, \quad (23)$$

$$T_{\text{damp}} \approx 0.008 \left[ \frac{0.1}{f_{\text{loss}}} \right] \left[ \frac{\rho}{1 \text{ g/cm}^3} \right] \left[ \frac{40 \text{ g/cm}^2}{\Sigma} \right] \left[ \frac{r_{\text{p}}}{1 \text{ m}} \right] \left[ \frac{a}{1.3 \times 10^5 \text{ km}} \right]^{3/2} \text{ yr}. \quad (24)$$

In the expression for the damping time, we adopt  $f_{\text{loss}} = 0.1$  (see §4.6).

Finally, the migration rates in the A ring, corresponding to equations (11–13), are:

$$\frac{da_{\text{emb}}}{dt} \lesssim -10^{-4} \left[ \frac{10 \text{ m}}{h} \right]^2 \left[ \frac{a}{1.3 \times 10^5 \text{ km}} \right]^{1/2} \left[ \frac{\Sigma}{40 \text{ g/cm}^2} \right] \text{ km/yr} \quad r_{\text{H}} \lesssim 2 \text{ km} \quad (25)$$

$$\frac{da_{\text{fast}}}{dt} \approx \pm 17 \left[ \frac{a}{1.3 \times 10^5 \text{ km}} \right]^{3/2} \left[ \frac{\Sigma}{40 \text{ g/cm}^2} \right] \text{ km/yr} \quad 2 \text{ km} \lesssim r_{\text{H}} \lesssim 24 \text{ km} \quad (26)$$

$$\frac{da_{\text{gap}}}{dt} \approx -0.009 \left[ \frac{r_{\text{H}}}{24 \text{ km}} \right] \left[ \frac{a}{1.3 \times 10^5 \text{ km}} \right]^{1/2} \left[ \frac{\Sigma}{40 \text{ g/cm}^2} \right] \text{ km/yr} \quad r_{\text{H}} \gtrsim 24 \text{ km}. \quad (27)$$

Equation (25) gives the maximum embedded rate for  $r_{\text{H}} \sim h$ , with the expectation that embedded satellites with larger radii cannot migrate faster as a result of viscous effects (e.g., D’Angelo et al. 2003). Equation (27) expresses the migration rate in the limit of small viscosity. In a viscous disk,

$$\frac{da_{\text{visc}}}{dt} \approx -3 \times 10^{-6} \left[ \frac{1.3 \times 10^5 \text{ km}}{a} \right] \left[ \frac{\nu_{\text{rad}}}{85 \text{ cm}^2/\text{s}} \right] \text{ km/yr} \quad r_{\text{H}} \gtrsim 24 \text{ km}, \nu_{\text{rad}} \gg 0. \quad (28)$$



These equations provide an idealized description of migration in the A ring. At small  $r_H$ , we take the embedded migration rate for  $r_H \sim 3h$  as a maximum value, since larger Hill radii are in the transgap regime where migration is likely suppressed. The large- $r_H$ , viscosity-dominated, Type II migration rate is formally below 1 cm/yr.

To put these results in perspective, we estimate the timescales for migration through a distance of 10,000 km, approximately half the annular width of the A ring:

$$\tau_{\text{emb}} \gtrsim 100 \left[ \frac{1 \text{ km}}{r_H} \right]^3 \left[ \frac{h}{10 \text{ m}} \right]^2 \left[ \frac{1.3 \times 10^5 \text{ km}}{a} \right]^{1/2} \left[ \frac{40 \text{ g/cm}^2}{\Sigma} \right] \text{ Myr} \quad r_H \lesssim 2 \text{ km} \quad (29)$$

$$\tau_{\text{fast}} \approx 0.0006 \left[ \frac{1.3 \times 10^5 \text{ km}}{a} \right]^{3/2} \left[ \frac{40 \text{ g/cm}^2}{\Sigma} \right] \text{ Myr} \quad 2 \text{ km} \lesssim r_H \lesssim 24 \text{ km} \quad (30)$$

$$\tau_{\text{gap}} \approx 1.1 \left[ \frac{24 \text{ km}}{r_H} \right] \left[ \frac{1.3 \times 10^5 \text{ km}}{a} \right]^{1/2} \left[ \frac{40 \text{ g/cm}^2}{\Sigma} \right] \text{ Myr} \quad r_H \gtrsim 24 \text{ km} . \quad (31)$$

$$\tau_{\text{visc}} \approx 370 \left[ \frac{85 \text{ cm}^2/\text{s}}{\nu_{\text{rad}}} \right] \text{ Myr} \quad (\text{viscous lifetime}) . \quad (32)$$

Figure 2 summarizes results for the migration rate in the A ring as a function of Hill radius. Satellites in or near the A ring are included in the diagram.

These timescales lead to several clear conclusions regarding migration through the A ring. Objects with Hill radii less than roughly 0.25 km migrate on a timescale comparable to the age of the solar system (see also Goldreich & Tremaine 1982, and references therein). This radius is roughly the maximum Hill radius of propeller moonlets in the A ring. Because the migration time scales as  $r_H^3$ , fast migration may be responsible for the lack of propeller moonlets with  $r_H \gtrsim 1$  km. Two moons, Pan and Atlas, have Hill radii very close to the fast migration cut-off  $r_{\text{fast}}$ . Although the predicted lifetimes for these moons are short compared to the age of the solar system, they are very long compared to the fast migration lifetime.

The small moon Daphnis clearly provides a more extreme challenge to migration theory. Its radius lies right in the middle of the expected range of radii for fast migration. With an expected migration time of less than 1000 yr, either (i) Daphnis is a recent addition to the rings, (ii) the migration theory is incorrect, or (iii) additional factors contribute to its apparent lack of migration. In the following sections, we address these possibilities and their impact on the rates shown in Figure 2.

#### 4. Migration of small moons: N-body experiments

To explore the migration of small moons through Saturn’s A ring in more detail, we examine a set of  $N$ -body calculations. To perform these calculations, we use *Orchestra*, a hybrid  $N$ -body-coagulation code which includes additional modules for the radial diffusion of gas and solid particles through a disk surrounding a star or a planet. In Bromley & Kenyon (2006), Kenyon & Bromley (2004, 2008, 2009), and Bromley & Kenyon (2011a), we describe each component of *Orchestra*, including comprehensive results with standard test problems. Here, we provide a short overview, with a focus on the  $N$ -body component, which we use exclusively in the calculations for this paper.

#### 4.1. N-body simulation method

The  $N$ -body algorithm distinguishes among three types of particles: the massive  $N$ -bodies, the “swarm” (superparticles), and the tracers. The massive  $N$ -bodies gravitationally interact with all particles in a simulation. The swarm particles interact with and can influence the motions of the massive  $N$ -bodies but do not interact with each other or with the tracers. The tracers respond to the gravity of the massive  $N$ -bodies. Here, we use massive  $N$ -bodies to track the motions of Saturn, its major moons, and the smaller moons. Unless noted otherwise, we represent the gravity of the ring using swarm particles. Thus, the ring is not self-gravitating.

*Orchestra* uses a 6<sup>th</sup>-order accurate symplectic integrator for all massive bodies in a computational domain that encompasses the full 3-D extent of all orbits. In the case of the relatively numerous tracer or swarm particles, a software switch allows for 4<sup>th</sup>-order accurate integration over a timestep that is typically 1/300<sup>th</sup> of the orbital period. During this step, the orbits of massive particles are interpolated in a way that allows them to respond to the gravity from swarm particles. The code handles close encounters with a massive body by solving Kepler’s equations. These features allow us to track up to  $10^8$  ring particles for thousands of orbits, or  $10^5$  ring particles for millions of orbits.

*Orchestra* can also accommodate rates of change in orbital elements, given by  $da/dt$  (semimajor axis),  $de/dt$  (eccentricity), and  $di/dt$  (inclination), from physical interactions among the swarm particles. Here, we use this feature to include the evolution of solid ring particles in a viscous disk. To calculate changes in these elements over a time step  $\Delta t$ , we use

$$\Delta a = \text{sgn}(u - 0.5) \sqrt{\nu_{\text{rad}} \Delta t} \quad (33)$$

$$\Delta e = -e \frac{\Delta t}{T_{\text{damp}}} \quad (34)$$

$$\Delta i = -i \frac{\Delta t}{T_{\text{damp}}} \quad (35)$$

where  $u$  is a standard uniform (pseudo)random variate used to implement a random walk to mimic the radial diffusion of the swarm particles. For individual isolated particles scattered within roughly a Hill radius of a small moon, the code has a switch to turn off this feature.

In the calculations for this paper, we chose a damping time of 0.01 yr, comparable to the predicted timescale in equation (24). The diffusion of small ring particles is an important aspect of the interactions between massive  $N$ -bodies and the swarm. As long as it is within an order of magnitude of our choice, the precise value of  $T_{\text{damp}}$  does not make any noticeable difference in the outcomes of our simulations,

To test this aspect of our  $N$ -body code, we considered the evolution of a narrow ring of small particles evolving solely by diffusion and collisional damping. Starting with initial conditions identical to Salmon et al. (2010), our simulations yield a gradual expansion of the narrow ring into a broad disk. For at least 100 Myr, the time evolution of the surface density distribution in our simulations closely follows Salmon et al. (2010), who solve the 1D radial diffusion equation for a disk of small particles. Comparisons with our own solutions to the radial diffusion equation further demonstrate that the  $N$ -body code treats particle diffusion and collisional damping accurately.

Finally, we developed and tested algorithms to model Saturn’s oblateness, which can significantly affect orbital phases and inferred orbital elements for all satellites and ring particles. When we include Saturn’s oblateness in the calculations, we set the gravitational acceleration at a distance  $\vec{x}$  near the ring to

$$\frac{d^2\vec{x}}{dt^2} = -\frac{GM}{x^3} \left[ 1 + 3J_2P_2(\sin\phi)\frac{R_S^2}{x^2} \right] \vec{x}, \quad (36)$$

where  $\phi$  is the latitude relative to the ring,  $P_2$  the second-order Legendre polynomial, and the gravitational constant  $J_2 = 0.01629$  for an adopted radius of Saturn  $R_S = 60,330$  km (Jacobson et al. 2006).

For this paper, we consider two sets of simulations. When examining a simple physical process – such as a small moon migrating through a pristine ring – we treat the dynamical interactions between a small moon and ring particles using swarm particles and the damping/viscous interactions among ring particles (eq. [35]), but we do not generally include the oblateness of Saturn or interactions with distant moons (e.g., Mimas, Rhea, Dione, etc). Eliminating oblateness and the distant moons allows us to investigate a larger range of input parameters per unit cpu time. Once we establish a typical behavior, we verify that including oblateness and interactions with distant moons do not change this behavior. In more complex simulations (e.g., for Daphnis in §5), we include oblateness and the interactions with distant moons and note the included moons in the text.

#### 4.2. Comparison with other techniques

The  $N$ -body algorithm in *Orchestra* differs from ‘patch’ simulations of Saturn’s rings, where the computational domain is a comoving rectilinear patch centered on a circular Keplerian orbit in the ring (e.g., Lewis & Stewart 2000; Porco et al. 2008; Salo & Schmidt 2010; Lewis et al. 2011; Perrine et al. 2011). Patch calculations include  $10^5$  to  $10^6$  ring particles with typical masses of  $5 - 10 \times 10^{-5}$  relative to the satellite of interest. For patches with sizes of roughly a square kilometer, these calculations can track the interactions and long-term evolution of ring particles with realistic sizes,  $\sim 1$ – $10$  m. To understand the origin of local structures within the rings, these calculations are ideal. However, periodic boundary conditions at the ‘ends’ of a patch limit the ability of these calculations to include perturbations from material outside the patch. Thus, it is challenging for these simulations to track the response of a moonlet or small moon to the global evolution of ring particles.

In *Orchestra*, the  $N$ -body code follows much larger particles,  $\sim 10$ – $100$  m, over complete orbits around the central mass. As long as the satellite mass exceeds the ring particle mass by a factor of a few hundred, calculations suggest that these superparticles can accurately represent smaller ring particles and their effect on an embedded satellite (Fig. 3 below; see also Kirsh et al. 2009). This approach also enables straightforward inclusion of resonances and other perturbations from distant moons. In our simulations, the number of superparticles is too small to identify small-scale or short-term structures within the ring particles. Thus, these calculations accurately follow the evolution of a small moon at the expense of a large graininess in the structure of the ring. Because our focus is on the long-term evolution of a satellite in response to the entire ring and distant

moons, this compromise is reasonable.

Although most previous  $N$ -body work has focused exclusively on ring particle dynamics, several studies consider radial drift of satellites within or outside the ring (Lewis & Stewart 2009; Charnoz et al. 2011; Tiscareno 2012). Despite their success in identifying sources of radial drift, none of these simulations can track fast migration. For example, Charnoz et al. (2011) elegantly track Type II-like migration by summing the torque on a moonlet at Lindblad resonances. However, the relevant part of the ring for fast migration is closer to the corotation zone than the Lindblad resonance (see Masset & Papaloizou 2003, for the analogous case of Type III migration in a gaseous disk). Thus, this approach will never yield fast migration.

Lewis & Stewart (2009) provide an excellent demonstration of chaotic drift of a moonlet by collisions and interactions with massive particles and self-gravitating wakes in the rings. However, their patch-like computational domain spans only a small fraction of a moonlet’s orbit around the planet. To produce fast migration in this type of calculation, we speculate that it is necessary to account for the phase and timing of a ring particle’s orbit when it reenters the patch. In all of their calculations, the moonlets of interest to Lewis & Stewart (2009) are too small to open the annular gap in the ring necessary for fast migration (e.g.,  $r_H < r_{\text{gap}}$ ). Thus, fast migration is not expected in any of their simulations.

### 4.3. Onset of fast migration

Sustained fast migration of a small moon requires one simple condition. The moon must be able to draw/scatter ring material from one edge of its corotation zone to the other and then drift a sufficiently large radial distance in the opposite direction to avoid encountering the scattered particles again. Moons that are too large cannot drift far enough before re-encountering scattered particles. Very small moons cannot clear enough of an annular gap and are inertially pinned by other corotating material at smaller orbital separation. Thus, moons which are too small or too large migrate very slowly.

Despite this clear picture for *sustaining* fast migration, *initiating* fast radial drift is more subtle. The onset of fast migration requires (i) a satellite with a fairly empty corotation zone and (ii) enough disk material close by, within  $\sim 3 - 4r_H$ , where dynamical interactions can draw material into the satellite’s corotation zone<sup>4</sup>. Among plausible starting points, we consider two extreme initial conditions, a satellite lying in a completely empty gap in the disk and a satellite embedded in a continuous disk.

Although a satellite within a continuous disk has enough material nearby to begin fast migration, it must first clear its corotation zone. For satellites with  $r_H \gtrsim r_{\text{gap}}$ , the timescale for scattering particles out of the corotation zone is smaller than the timescale for viscous diffusion to bring particles back into the corotation zone. Thus, the satellite begins to clear its corotation zone

---

<sup>4</sup>In addition to particles on horseshoe orbits, material on initially circular orbits with  $\Delta a$  as large as  $2\sqrt{3}r_H$  can be deflected onto crossing orbits with the satellite (Gladman 1993).

(see also Lissauer et al. 1981; Hourigan & Ward 1984; Rafikov 2001). Whether or not the satellite drifts slowly in the type I mode, any imbalance in the net amount of scattering into the inner disk relative to the outer disk creates a net drift sufficient to begin fast migration. As long as the physical properties of the disk and the satellite maintain the conditions  $T_{\text{clear}} \gtrsim T_{\text{fill}}$  and  $r_{\text{H}} \lesssim r_{\text{fast}}$ , the satellite continues fast migration.

For a satellite within a large gap, the onset of fast migration is more delicate. Despite its empty corotation zone, the satellite must reach across the gap and draw material from the gap edges into the region,  $\Delta a \lesssim 2\sqrt{3}r_{\text{H}} \sim 3.5r_{\text{H}}$ , where orbit crossings can begin. For a satellite with  $r_{\text{H}} \gg r_{\text{fast}}$ , the half-width of the gap is much larger than  $\sim 3.5 r_{\text{H}}$ . Disk material is too far away; the satellite can only migrate in the type II mode. For satellites with  $r_{\text{gap}} \lesssim r_{\text{H}} \lesssim r_{\text{fast}}$ , the edges of the gap are within  $\sim 3.5 r_{\text{H}}$ . Material can then be drawn into crossing orbits with the satellite.

Although satellites with  $r_{\text{gap}} \lesssim r_{\text{H}} \lesssim r_{\text{fast}}$  have fairly small gaps, it is possible to construct a disk where orbit crossings never occur. We first consider a disk where the surface density at the inner edge of the gap is comparable to the surface density at the outer edge. When (i) a disk has a vertical scale height  $h \equiv 0$ , (ii) the satellite lies on a perfectly circular orbit centered in a gap with half-width  $\Delta a \gtrsim 4r_{\text{H}}$ , and (iii) there are no external torques, the torque balance between the satellite and the gap edges is perfect (e.g., Hourigan & Ward 1984). The satellite cannot draw material into its corotation zone and can only migrate slowly in the type II mode.

In a real disk, the finite scale height breaks the symmetry, allowing the satellite to draw material from the gap edges (Hourigan & Ward 1984). Once the satellite begins to draw material from the edges of the gap across its corotation zone, additional jostling of the gap edges or the satellite’s orbit – for example, by density fluctuations in the disk or by gravity fluctuations due to distant moons – places the satellite closer to material at one edge of the gap than the other edge. The satellite draws more material into its corotation zone. Fast migration commences.

To try to maintain the satellite on a stable orbit, we can specify the surface density on the inner/outer edges of the gap to balance the slightly different angular momenta of particles on either edge of the gap. We can also specify that the number of orbit crossings from material in the inner disk precisely balance the number from the outer disk. Every ensemble of scattering events then leads to no radial motion. Neglecting internal ring dynamics and other external processes, the satellite can maintain a wide, clear gap and remain on its initial orbit indefinitely.

In a real ring, however, this balance is metastable. Radial diffusion tries to fill the gap. Perturbations from scattering by self-gravitating wakes, direct collisions, or asymmetries in the Type I-like torques (eq. [11]) from more distant ring material pushes ring particles into the gap (e.g., Tiscareno 2012). Jostling by distant moons also tends to fill the gap. If these processes fill both sides of the gap identically, it is possible to maintain the balance. If these perturbations leave a few extra particles on one edge of the gap, the additional crossing events will pull the moon in that direction. Once the moon is drawn to either gap edge, it will pull even more particles from that edge, enhancing its radial drift. Fast migration again commences.

To explore these two possibilities in more detail, we examine a suite of numerical simulations for satellites in disks with physical characteristics similar to Saturn’s A ring. We begin with a

discussion of fast migration for a satellite in a completely empty gap. We then consider a satellite in a continuous disk.

#### 4.3.1. *Fast migration in smooth rings*

To illustrate metastability of a satellite in a pristine gap, we set up an initially stable configuration with balanced torques from either edge of the gap. The simulations consider two plausible initial conditions for particles spaced uniformly in radius through the ring: particles spaced (i) randomly or (ii) uniformly in the azimuthal direction. The calculations also consider two types of ring particles: (i) massive swarm particles, where we calculate the radial drift from individual  $N$ -body interactions directly or (ii) massless tracer particles, where we derive the drift from the change in the total angular momentum of the tracers. This approach allows us to test the sensitivity of the migration rate to the initial orbits of ring particles and to the method for calculating torques between the moon and ring particles.

For a small moon with  $r_H = 7$  km and a gap with half-width  $= 2 r_H$ , fast migration initiates in every simulation in this suite of tests (Fig. 3). Moons interacting with tracer particles tend to begin migrating earlier than moons surrounded by massive swarm particles. Moons within a random distribution of ring particles appear to start migrating earlier than moons in a uniform distribution. In all cases, the onset of fast migration requires a short time, smaller than the synodic period of material at the gap edge. When the mass ratio of the moon to a ring particle is large,  $> 10^3$ , the onset is slow and regular. When the mass ratio is  $\lesssim 10^2$ , migration is more stochastic and start more quickly due to individual scattering events that push the moon toward the edge of the gap. Still, both sets of initial conditions, both approaches to calculate the radial drift, and all mass ratios yield roughly the same migration rate.

To explore the onset of fast migration in more detail, we conducted additional tests with larger gaps and different diffusion timescales. The range of gap sizes, with half-widths  $\Delta a$  from  $2r_H$  to  $6r_H$ , includes two nominal half-widths that are important from gap-formation theory (see the Appendix): the first is  $\Delta a \approx 3r_H$ , derived by balancing torques between the satellite and the disk (Lissauer et al. 1981), while the second is  $\Delta a \approx 2.5r_H$ , derived by balancing scattering with viscous diffusion. In all these tests, ring particles slowly diffuse into the gap. The width of the gap around the moon gradually decreases. With the nominal diffusion time of 10 yr for a small, gap-clearing moon, larger gaps fill in more slowly, and imply longer times before migration can start. When the gap width closes to roughly twice the corotation half-width,  $\Delta a \approx 4r_H$ , the moon starts to chaotically scatter ring particles. Fast migration then ensues. With no diffusion, large gaps remain pristine. Although slow, type I torques can cause radial drift on very long timescales, fast migration cannot begin until the moon is within a corotation radius of either edge of the gap. Therefore, eliminating particle diffusion in a large gap effectively eliminates fast migration.

### 4.3.2. Fast migration in wide gaps: encroaching ring edges

To provide more details on how a moon within a large gap begins fast migration, we consider another example. The simulation begins with a small moon,  $r_{\text{H}} = 4.9$  km, in a perfectly circular orbit within a large gap of half-width  $\Delta a = 20$  km  $\approx 4r_{\text{H}}$ . The gap is centered within a larger ring of particles with properties appropriate for the A ring, equations (14–16). As in other calculations, ring particles have a diffusion time of 10 yr. The simulation spanned more than 50 years, or 25,000 orbits. A sequence of snap shots shows how gap edges are sculpted and how particle orbits diffuse close enough to the satellite to trigger fast migration.

Figure 4 illustrates how ring material slowly diffuses into a wide gap and eventually leaks onto orbits that interact strongly with the small moon. Before the moon starts to migrate, very little of this material enters the moon’s corotation zone. Instead, slight imbalances draw the moon slightly closer to one gap edge than the other. This process is slow. In the top two panels of Figure 4, the time difference is roughly 40 yr. Only slight changes are visible. The gap is still well defined. The wakes created by the moon are clear.

Once changes begin, they are rapid. In Figure 4, the lower two panels show the scene only a few years later. Orbit crossing is rampant. As the moon drives into one side of the gap, it pulls material across, opening a new gap ahead of it and filling in the space behind it. This new, smaller and less well-defined gap comoves with the satellite (see Bromley & Kenyon 2011b, and the associated animation in a much broader disk). Although the original gap remains behind, viscous diffusion slowly fills it in.

Tests with moons of other sizes in gaps of varying widths yield similar results. Diffusion tries to fill the gap; scattering tries to empty it. Eventually, there is an imbalance which pushes the moon towards one edge of the gap. The accelerating imbalance between scattering and viscous diffusion allows the moon to draw more and more material from the gap and to move closer and closer to the edge of the gap. Once the imbalance reaches a critical level, fast migration begins.

The starting conditions for the results shown in Figure 4 are *almost* a realistic representation of Daphnis, the A ring and the Keeler gap. The single difference is the initial orbit of the moon. In the simulation, the initial orbit has  $e = i = 0$ . The real orbit is slightly eccentric and inclined to the ring plane. As we show in §5, the time required for a moon to begin fast migration depends on the initial  $e$  and  $i$ . However, the overall outcome is identical: the moon always begins fast migration.

### 4.3.3. In situ formation and clearing the corotation zone

When it grows by coagulation/accretion, a satellite forms within a dense disk of particles. With a full corotation zone, this satellite cannot migrate in the fast mode. Previous numerical experiments (e.g., Kirsh et al. 2009) demonstrate that a satellite can gravitationally scatter away enough of the corotating material to trigger fast migration in a particle disk. Here, we illustrate the same phenomenon for a small moon in Saturn’s A ring. Figure 5 shows results for a simulated moon with  $r_{\text{H}} = 14$  km in the A ring. The figure tracks the orbital distance and the amount of material in the corotation zone as a function of time. After the mass in the corotation zone falls

to about a third of its starting value, fast migration starts. The mass of corotating material then peaks up as the moon plows through fresh material during its inward spiral through the disk.

Figure 5 shows that a small moon rapidly clears its corotation zone (for other examples of this phenomenon, see also Rafikov 2001; Kirsh et al. 2009). Within 10–20 yr, gravitational scattering removes roughly half the mass of the corotation zone. During this period, the moon slowly moves radially inward and outward in response to perturbations from swarm particles in the corotation zone. After  $\sim 100$  yr, the moon has removed enough material from the corotation zone to begin fast migration. After migrating inward roughly 200 km, the moon’s progress is halted as it encounters the edge of the disk.

Our simulations demonstrate that this behavior is independent of the general background perturbations from other small moons and larger distant ones orbiting Saturn. Comparison of calculations without distant moons (Fig. 5, black curve) and with a full complement<sup>5</sup> of moons (Fig. 5, grey curve) shows modest differences resulting from stochastic variations in the orbits of swarm particles but no large variation in the timing or rate of migration. Results for a large suite of simulations yield the same conclusion: fast migration of satellites with  $r_{\text{gap}} < r_{\text{H}} < r_{\text{fast}}$  is a robust phenomenon in the A ring. Thus, the general lack of small moons in the ring is consistent with migration theory (see also Goldreich & Tremaine 1982).

#### 4.3.4. *Orbital settling into a ring*

The onset of fast migration depends on the initial orbital parameters of a satellite. When a small moon is scattered into an otherwise unperturbed region of a ring, it will probably have a large orbital eccentricity or inclination relative to the ring particles. The moon then tries to clear a region much larger than its corotation zone. When  $e \gtrsim 10^{-5}$ , the radial excursion of the moon exceeds the radius of its corotation zone. When  $i \gtrsim 10^{-7}$ , the moon spends most of its time outside the ring and cannot completely clear out material along its orbit. However, gravitational interactions with the ring particles damp  $e$  and  $i$  (e.g., Goldreich & Tremaine 1981; Borderies et al. 1984; Ward 1988; Hahn 2007, 2008). Once  $e$  and  $i$  are small, the moon can clear its corotation zone and begin fast migration.

To derive the damping time for a small moon with an inclined orbit, we perform a set of calculations with various initial  $e$  and  $i$  relative to swarm particles in the A ring. Figure 6 illustrates the rapid damping of  $e$  and  $i$  experienced by a small moon in a typical calculation. For moons capable of undergoing fast migration, the damping timescale is well within 1–2 decades. The inclination damps smoothly and reaches  $i < 10^{-6}$  in 10–20 yr. After moons reach  $e < 10^{-4}$ , the drop in  $e$  is more gradual and includes additional stochastic variations due to perturbations in the surface density of swarm particles.

Once a small moon achieves a nearly circular orbit, the timescale to damp the orbit further is

---

<sup>5</sup>In these simulations, a ‘full complement’ of moons includes the ring moons Pan, Daphnis, Atlas, Prometheus, Pandora, Epimetheus, and Janus and the larger, more distant moons Mimas, Enceladus, Tethys, Dione, Rhea, Titan, and Iapetus.



much longer. When the inclination satisfies  $r_{\text{H}} \lesssim ai$ , the moon can begin to clear its corotation zone. The timescale to reach this inclination is roughly the viscous time to fill the gap formed when the moon had much larger  $e$  and  $i$ . Figure 7 provides an illustration. A small moon, with  $r_{\text{H}} = 6.5$  km, experiences a slow damping followed by a transition to fast migration.

Simulations of the orbital evolution of small moons with  $r_{\text{gap}} < r_{\text{H}} < r_{\text{fast}}$  and a broad range of starting  $e$  and  $i$  yield similar results. As the moons try to clear a gap much larger than their corotation zones, their  $e$  and  $i$  damp. While  $e$  and  $i$  damp, viscous spreading fills in the gap outside a moon’s corotation zone. After  $i$  reaches a threshold, fast migration begins.

The vertical scale height of the ring sets the threshold for fast migration of a small moon with an inclined orbit relative to the ring. The condition for fast migration is  $i_{\text{fast}} < r_{\text{H}}/a$ . When  $i \gtrsim r_{\text{H}}/a$ , moons cannot completely clear their corotation zones before viscous spreading fills them in. After damping reduces  $i$  to the threshold  $i_{\text{fast}}$ , fast migration begins.

We conclude that fast migration may be a common, if not ubiquitous, process in a disk similar in structure to Saturn’s A ring. The migration time is extremely short compared to the  $\sim 0.1$ – $1$  Gyr lifetime of the ring (e.g., Esposito 2010). Thus, (i) all moons with  $r_{\text{H}} \gtrsim r_{\text{gap}}$  are recent additions to the ring or (ii) physical structures within the ring prevent migration. To address these possibilities, we next consider how density perturbations within the ring impact migration. In §5, we examine the possibility that the moons are young.

#### 4.4. Fast versus stochastic migration

The A ring is dynamically active, with a variety of long-lived and transient physical structures. Many features are associated with spiral density waves (e.g., Cuzzi et al. 1981) or bending waves (e.g., Shu et al. 1983). In addition to the surface density enhancements immediately surrounding moonlets (the propellers), nearby moonlets or small moons generate gravitational wakes in the rings (Showalter et al. 1986). Additional variations of optical depth in the A ring result from self-gravity wakes (Hedman et al. 2007), which vary in structure across orbital resonances with Saturn’s moons.

Although simulating the full range of structure present in the A ring is beyond the current capabilities of *Orchestra*, we can establish how a variety of density perturbations impact fast migration in the A ring. We begin with simulations designed to illustrate how clumpiness in the ring impacts migration.

Figure 8 shows a suite of simulations of a moon with  $r_{\text{H}} = 14$  km at an orbital distance of 130,000 km embedded in rings with a fixed surface density and with swarm particles of various sizes. The swarm particles in each simulation all have the same mass, but from run to run, that mass ranges from 0.2% to 10% of the moon mass. In all simulations, the corotation zone is initially free of disk particles in an annulus of  $3r_{\text{H}}$ . Fast migration begins nearly immediately. Without this initial clearing of the corotation zone, there is a time lag  $\sim T_{\text{clear}}$  in the onset of fast migration (see Fig. 5 and Kirsh et al. 2009).

These simulations demonstrate that density perturbations can change migration rates substantially. As the mass of a swarm particle increases, migration through the ring becomes more and

more erratic (Fig. 8). When swarm particles are 10% of the satellite mass, migration begins to resemble a random walk process, as envisioned in the stochastic migration scenario of Crida et al. (2010, see also Tiscareno 2012).

For a more detailed illustration of discreteness effects in migration, we consider the migration of a small moonlet with  $r_H = 700$  m. As in Figure 5, the calculations include all of Saturn’s major moons (e.g., Titan and Rhea) and smaller moons near the A ring (e.g., Prometheus and Pandora). To enable computational feasibility, we reduce the number of swarm particles by decreasing the surface density of the A ring by a factor of 100, setting the mass of swarm particles at 1–2% of the moonlet mass, and clearing the corotation zone of swarm particles. We also turn off viscous diffusion. Without viscosity, particles with Hill radii comparable to the propeller moonlets ( $r_H \lesssim 1$  km) can maintain a fairly empty corotation zone once they start migrating.

Figure 9 shows typical results of these simulations. The noisy horizontal curve in light grey measures the fluctuations in semimajor axis – as measured in a reference frame centered on Saturn – of an isolated moonlet orbiting the planet but not migrating through the disk. These fluctuations result from the constant gravitational jostling from distant and nearby moons. When the moonlet is allowed to migrate (as in the black and dark grey curves, which have particles that are 1% and 2% of the moonlet mass, respectively), its semimajor axis shifts in a stepwise fashion which tracks the theoretical prediction (dashed curve). Over a one year time frame, the total migration is comparable to the variation in  $a$  from jostling by distant moons.

These two simulations illustrate the difficulty of measuring migration rates in Saturn’s rings and other complex systems. Gravitational jostling of orbits by distant moons is comparable to the expected radial excursions of small moonlets comparable in size to Blériot and other propellers in the rings. Interactions with larger ring particles can hinder or reverse migration of a larger moon on short timescales (e.g., Tiscareno 2012). In all cases, measuring robust migration rates requires long time baselines and stable reference frames.

#### 4.5. Migration in the presence of distant moons: resonances

In addition to propellers and wakes, Saturn’s moons create a variety of structure within the A ring. The moons Pan (Encke gap) and Daphnis (Keeler gap) lie within distinct low density gaps within the rings. A 7:6 resonance with the coorbiting moons Janus and Epimetheus is responsible for the outer edge of the A ring (e.g., Lissauer et al. 1985). The “ring moons” Atlas, Pandora, and Prometheus just outside the ring also produce structure in the ring.

To illustrate the rich set of other resonances in the A ring (see also Lissauer & Cuzzi 1982), Figure 10 shows the result of a simulation of 10,000 tracer particles orbiting Saturn along with the major moons (Mimas, Enceladus, Tethys, Dione, Rhea, Titan, and Iapetus) and several smaller moons much closer to the ring (Pan, Daphnis, Atlas, Prometheus, Pandora, Janus and Epimetheus). Ring particles have large maxima in  $e$  around Pan (the Encke gap) and at the outer edge of the ring (the 7:6 resonance of Janus and Epimetheus). Other rises in  $e$  occur at the orbits of Atlas and Prometheus – which lie beyond the outer edge of the ring in regions of very low surface density – and at many other labeled resonances. Several of these resonances lie close to but are not obviously

coincident with the orbit of Daphnis within the Keeler gap. Curiously, a large ensemble of propeller moonlets lie between the 5:4 resonance of Janus/Epimetheus and the 5:3 resonance with Mimas.

To explore the impact of orbital resonances on migration, we consider whether small moons can pass through the 5:4 resonance with Janus and Epimetheus. We set up an ensemble of moons with  $r_{\text{H}} = 3\text{--}15$  km on either side of the resonance near  $a = 130,500$  km. Because small moons can migrate inward or outward, some moons attempt to migrate across the resonance. Others try to migrate away from the resonance. In all cases, Janus/Epimetheus stir up the eccentricities of ring particles close to the resonance. Large vertical scale height and large eccentricity are barriers to fast migration. Thus, we expect the migration of smaller moons to stall close to resonance.

The results in Figure 11 confirm our expectations. Resonant interactions with Janus and Epimetheus stir up enough ring material to create an obstacle for smaller moons. Moons with  $r_{\text{H}} = 3.5$  km do not cross the “barrier” set up by the 5:4 resonance. However, moons with  $r_{\text{H}} = 14$  km migrate right through the resonance.

To understand this resonant barrier to migration, we examine the eccentricity of ring particles close to and far away from the resonance. At resonance, Janus and Epimetheus can stir ring particles to fairly high eccentricity ( $e_{\text{p}} \sim 10^{-5}$ ; see Fig. 10). Away from resonance,  $e_{\text{p}}$  is a factor of  $\gtrsim 10$  smaller. At a distance of 130,000 km from Saturn, these ring particles have radial excursions of a few kilometers. When they are at resonance, small moons or moonlets with Hill radii smaller than a few km are thus embedded in a dynamically hot ring, which dramatically reduces their migration rate (Bromley & Kenyon 2011a, eq. 21). Moons with Hill radii larger than a few km lie in a dynamically cold ring whether or not they are within the resonance. These larger satellites migrate freely.

The value of  $r_{\text{H}}$  that separates these two modes of migration through a resonance depends on several factors. With other properties of the rings held fixed, stronger (weaker) resonances produce stronger (weaker) eccentricity enhancements, creating barriers for larger (smaller) moons. If the strength of the resonance is held fixed, stronger (weaker) damping or viscous spreading weakens (strengthens) eccentricity enhancements, enabling (preventing) migration. Thus, understanding barriers to migration requires a thorough understanding of the physical processes that impact the eccentricity of ring particles.

#### 4.6. Migration in the presence of distant moons: stirring

Although distant moons outside of resonance weakly stir the eccentricity and inclination of ring particles, this stirring can have a major impact on the structure of the rings. Using the impulse approximation, Weidenschilling (1989) showed that distant moons give a particle a small kick in  $e$  and  $i$  every synodic period. For an ensemble of distant moons, he derived a stirring rate

$$\frac{de^2}{dt} \sim \sum_n \frac{m_n^2}{M^2} \frac{a^3}{|a - a_n|^3} \frac{1}{T}, \quad (37)$$

$$\frac{di^2}{dt} \sim \sum_n \frac{m_n^2}{M^2} \frac{(i^2 + i_n^2)a^5}{|a - a_n|^5} \frac{1}{T}, \quad (38)$$

where  $m_n$ ,  $a_n$  and  $i_n$  are the mass, orbital distance and inclination of the  $n^{\text{th}}$  moon. These expressions are valid for objects on nearly circular orbits.

For the Saturn system, this approach is valid for moons with separations from the ring,  $\delta a$ , much smaller than the semimajor axis of ring particles. Thus, these equations apply to moons as far as Janus and Epimetheus (and possibly Mimas), but are invalid for more distant moons (e.g., Titan). With an orbital distance of  $1.2 \times 10^6$  km, Titan tugs more on the barycenter of the entire saturnian system instead of stirring the rings.

Our calculations yield results in rough agreement with the analytic theory. In several simulations for Figure 10, the eccentricity of ring particles grows at a rate  $de^2/dt \sim 10^{-11} \text{ yr}^{-1}$ , within a factor of two of the prediction from eq. (37). With typical  $e \lesssim 10^{-6}$  for ring particles, the growth time for stirring by distant moons is a fraction of a year, roughly equivalent to the damping time.

To compare stirring by distant moons with collisional damping in more detail, we consider the energy involved in both mechanisms. Stirring by distant moons results in a kinetic energy input per unit mass of  $\mathcal{P}_{\text{stir}} \sim v_{\text{Kep}}^2 de^2/dt \sim 2 \times 10^{-7} \text{ dyne g}^{-1}$ . The power per unit mass dissipated by collisions is

$$\mathcal{P}_{\text{coll}} \sim \frac{\Sigma}{m_p h} v_p \pi r_p^2 f_{\text{loss}} m_p v_p^2 \quad (39)$$

$$\sim 6 \times 10^{-7} \text{ dyne/g}, \quad (40)$$

where  $m_p$  is the characteristic mass of the ring particles. To derive this estimate, we adopt ring particles with  $r_p = 1 \text{ m}$  and  $\rho_p = 1 \text{ g cm}^{-3}$ . The rough equality of these rates suggests that the A ring’s velocity dispersion and thickness are supported by stirring from distant moons. A precise balance between the two energies requires modest changes in the size/density of the ring particles.

To examine the impact of stirring by distant moons in more detail, we consider simulations of a single ring particle interacting with Mimas, the innermost massive moon of Saturn. Each calculation begins with a ring particle orbiting at  $a \approx 136,500 \text{ km}$ , with  $e \approx 3 \times 10^{-5}$  and  $i \approx 6 \times 10^{-5}$  relative to the ring plane<sup>6</sup>. Mimas begins at a random phase in its orbit, which is tilted by roughly  $1^\circ$  relative to the ring plane.

Figure 12 shows the results. In a basic set of simulations, Mimas rapidly stirs the  $e$  and  $i$  of the ring particle (left panels of figure). The growth rate of  $e$  follows the Weidenschilling (1989) estimate closely. The growth rate of  $i$  is several times faster than predicted. In these simulations, a distant perturber (Mimas) continuously forces the alignment of angular momentum vectors between Mimas and the ring particle. Thus, the impulse approximation fails and  $i$  grows rapidly. Although adding collisional damping slows the growth of  $e$  and  $i$  (right panels),  $e$  and  $i$  still grow rapidly.

When we introduce the oblateness of Saturn into these simulations, the growth of  $e$  and  $i$  stalls. In the gravitational field of an oblate Saturn, the ring particle precesses rapidly. Because the precession time is short compared to Mimas’ orbital period, Mimas cannot force alignment of angular momenta. Thus, a single ring particle maintains a constant  $e$  and  $i$  (Fig. 12, left panels,

---

<sup>6</sup>These elements are similar to those of Daphnis.

light grey lines). Reducing the precession rate by a factor of 100 enables Mimas some impact on the ring particle;  $e$  and  $i$  then vary periodically (Fig. 12, left panels, dark grey lines).

Including damping and oblateness into the calculations produces a different equilibrium between stirring and damping. With a reduced precession rate (Fig. 12, right panels, dark grey lines),  $e$  and  $i$  oscillate about a slowly declining median level. With a normal precession rate around an oblate Saturn,  $e$  and  $i$  decline monotonically (Fig. 12, right panels, light grey lines). At late times,  $t \gg 10^2$  yr,  $e$  and  $i$  settle into an equilibrium with  $e \approx i \approx 10^{-7} - 10^{-6}$  set by the damping rate. Larger damping results in a smaller equilibrium  $e$  and  $i$ .

This suite of simulations demonstrates that a balance between damping and stirring by distant moons sets an equilibrium  $e$  and  $i$  for ring particles. Throughout the ring, the damping time grows in regions of reduced surface density (eq. [8]). Thus, stirring by distant moons is more important in regions of low surface density. Because migration slows in regions with large  $e$  and  $i$ , stirring by distant moons can inhibit migration more easily in regions of low surface density.

## 5. Daphnis

If the migration theory outlined in §2 is correct, the A ring should contain no moon or moonlet larger than a few kilometers. Larger satellites migrate to the ring edges on timescales much shorter than the ring lifetime. Although some smaller moonlets – like the propellers – can migrate slowly, our simulations show that they cannot pass through modest resonances. Aside from Daphnis, the ring has no large moonlets or small moons capable of migrating through the resonances shown in Figure 10. Because Daphnis should migrate so swiftly, understanding the origin and the behavior of Daphnis is essential to migration theory.

With an orbital distance of 136,505 km from Saturn, Daphnis is embedded in the  $\sim 20$  km wide Keeler gap (Weiss et al. 2009). It has a modest eccentricity  $e \approx 3 \times 10^{-5}$  and inclination  $i \approx 6.3 \times 10^{-5}$  (Jacobson et al. 2008). Relative to a circular orbit in the ring plane, the radial and vertical excursions of Daphnis have amplitudes of roughly 10 km, about twice the moon’s Hill radius of 4.9 km (Thomas 2010).

Daphnis is a mystery. Despite having a Hill radius within the range identified for fast migration, its radial drift is negligible. Using the measured viscosity of the A ring (e.g., Tiscareno et al. 2007; Colwell et al. 2009), the timescale for ring particles to circularize Daphnis’ orbit is  $\sim 1500$  yr (eq. [7]; see also Hahn 2008). Reducing the inclination to zero follows soon thereafter (see also Hahn 2007), allowing fast migration to commence. With an expected total lifetime in the interior of the A ring,  $\sim 2500$  yr, much shorter than the age of the rings, migration models are closely linked to models for the origin of Daphnis.

### 5.1. Origins

There are three possible origins for Daphnis. If this small moon is a recent addition, it might be a fragment produced during the impact of a comet or an asteroid with the ring system. Al-

ternatively, it might have formed *in situ*. We reject the idea that the moon results from a three (or more) body interaction with Saturn’s major moons and outer irregular satellites. The escape velocities of Saturn’s moons are too low to scatter the moon into the rings. If the current orbit of Daphnis is stable for timescales much much longer than the  $\sim 1000$  yr migration time, Daphnis is a much older resident of the rings, perhaps a remnant of the tidal event that produced the ring system. In this scenario, some set of external processes prevents Daphnis from migrating. To judge which of these possibilities is more likely, we consider each in more detail.

Although there is a low probability that Daphnis is an impact fragment (e.g., Cuzzi & Durisen 1990), this scenario is easy to test with observations. The current orbital eccentricity and inclination are appropriate for a small moon settling into the ring (Fig. 6). The numerical simulations demonstrate that  $e$  and  $i$  damp to zero on timescales of 100–1000 yr (see also Hahn 2007, 2008). For Daphnis’ orbit in the A ring, we expect the maximum altitude above the ring to decrease by 10–100 meters per year. Although there are no current observational limits on this rate, a direct measurement would constrain this ‘recent external origin’ scenario.

Forming Daphnis *in situ* is more likely. Charnoz et al. (2010, 2011) show that many of the inner moons of Saturn may have grown from ring material. Although Daphnis lies inside the orbits of the moons considered in Charnoz et al. (2010), it is reasonably close to the outer edge of the A ring. If Atlas, Prometheus, and other larger moons formed just outside the ring, it is reasonable to suppose Daphnis formed with them and migrated inwards to its present location.

Despite the attraction of this idea, Daphnis’ current orbit still requires special timing. The size of the Keeler gap surrounding Daphnis’ orbit is roughly the correct size for a gap produced by a moon like Daphnis. If Daphnis cleared this gap, then it should migrate on short timescales (Fig. 5). Thus, for *in situ* formation to be viable, it probably happened relatively recently.

Although this conclusion seems at odds with the Charnoz et al. (2010) simulations, observations can test this ‘recent in situ origin’ scenario. Because changes in altitude above the rings and the radial motion of Daphnis are detectable, direct measurements can establish whether the orbit of Daphnis is damping vertically or migrating radially.

Because these scenarios seem so unlikely, we consider other processes that might prevent rapid migration of Daphnis. As shown in the simulations for Figure 11, distant moons may establish a resonant barrier which prevents radial migration. In a cursory search for candidates, the Prometheus 32:31 and Pandora 18:17 resonances seem promising. Although the chaotic behavior of the orbits of Saturn’s inner moons complicates measuring the strength of resonances and their impact on Daphnis, our simulations demonstrate that resonances can stop the radial migration of moons similar to Daphnis.

Gravitational stirring by distant moons may also prevent migration (Fig. 12). Several of the larger moons – notably Mimas and Tethys – have orbits with inclinations  $i \approx 1^\circ$  relative to the ring plane. Mimas and Tethys are also locked in a 2:4 mean motion resonance (e.g., Allen 1969; Vienne & Duriez 1992; Champenois & Vienne 1999). Stirring by Mimas and Tethys counter viscous damping by the rings. From equations (37)–(38), we estimate that Mimas doubles the eccentricity of Daphnis in less than a decade. With its larger mass, Tethys can double Daphnis’ eccentricity

in 1.5 yr. Because these timescales are comparable to the damping time, stirring plausibly slows down migration.

## 5.2. Simulations

To test the two possibilities to halt Daphnis’ migration in more detail, we turn to a set of numerical calculations. Currently, we cannot simulate the full set of physical processes which impact Daphnis’ orbit. Our goal is to show that resonances and stirring by more distant moons are plausible mechanisms to prevent migration in Daphnis.

We begin with a suite of test runs for a single moon with the Hill radius of Daphnis embedded within the Keeler gap. Starting from Daphnis’ current  $e$  and  $i$ , the moon rapidly aligns with the ring (Hahn 2007, 2008). With a roughly linear decrease in the vertical excursion of Daphnis of about  $50 \text{ m yr}^{-1}$ , Daphnis’ maximum height above the ring plane drops from  $\sim 10 \text{ km}$  to much smaller than  $1 \text{ km}$  in roughly 200 yr (Fig. 13). Once Daphnis has a vertical amplitude smaller than the scale height of the ring, it begins fast migration.

For the next set of simulations, we consider a Daphnis-sized moon in the 32:31 resonance with Prometheus. The resonance pumps up the eccentricity and then maintains a roughly sinusoidal variation in  $e$  for  $\sim 10 \text{ yr}$ . As  $e$  oscillates, the resonance pushes the moon outside the gap. Once the moon lies within pristine ring material, damping dominates stirring by the single outer moon. Both  $e$  and  $i$  decline dramatically. When  $i$  falls below the threshold  $i_{\text{fast}} < r_{\text{H}}/a$ , the moon commences fast migration (Fig. 13, light grey line).

Moving Daphnis from the Prometheus 32:31 resonance to the Pandora 18:17 resonance leads to similar behavior on longer timescales. Within the Pandora resonance, Daphnis’ orbit remains inside the Keeler gap for  $\sim 20 \text{ yr}$ . The resonance then moves Daphnis out of the gap into the ring. Although it takes awhile for the ring to damp Daphnis’ inclination,  $i$  eventually drops below  $i_{\text{fast}}$ . Daphnis then begins fast migration.

When we move Daphnis’ orbit to an off-resonance location, its orbit becomes more stable, at least on decade-long time scales (Fig. 13, light grey line). In this set of calculations, Daphnis settles into the ring on a time scale comparable to calculations without Prometheus and Pandora, or perhaps even faster. There is no clear sign that stirring from these small, nearby moons can prevent settling. However the moons do cause some small differences in the evolution of orbital elements, which is an encouraging sign: during the first 5000 simulated orbits (7.5 yr), Daphnis’ inclination shows very little damping.

These simulations demonstrate the ability of interactions with the distant moons to affect the orbital parameters of Daphnis-sized moons on very short timescales. Finding plausible equilibria for Daphnis within the Keeler gap requires a detailed parameter search to identify the best combination of initial  $(a, e, i)$  for the satellite and the outer moons, and  $(\Sigma, \nu_{\text{rad}}, T_{\text{damp}})$  for the ring. Although several test simulations suggest it is possible to find equilibria stable over million year timescales, the computational effort is significant and beyond the scope of this paper.

In a final set of simulations, we consider the reaction of Daphnis to non-resonant interactions

with all of the distant moons. The simulations with Mimas in §4.5 show that a balance between damping and stirring from a single moon can maintain a large inclination, with  $i \gtrsim i_{fast}$ . Stirring by Prometheus and Pandora can reduce settling rates, at least over several thousand orbits. Thus, stirring from all the outer moons could maintain a large inclination, probably with some jitter due to the constantly changing gravitational field along Daphnis’ orbit.

As in Figure 10, these simulations include all of the major moons and the ring moons. The coordinates of the moons and Daphnis relative to Saturn come from the JPL Horizons systems (Giorgini et al. 1996) 00:00:00 GMT, 2012-June-22; we adjusted the ring plane to enable starting conditions for Daphnis similar to those in Figure 13. The calculations include the A-ring with an empty Keeler gap, damping and diffusion of ring particles, and Saturn’s oblateness.

Figure 14 shows the results of one simulation. As in Figure 13, the thin black curve shows the decay of  $e$  and  $i$  of a lone Daphnis orbiting within the Keeler gap and interacting only with ring particles. Orbital interactions with the full ensemble of Saturn’s moons yields relatively rapid, small amplitude fluctuations in  $a$  and  $e$ . This jitter is similar in amplitude to the jitter of any small moon in the ring (see Fig. 9). On much longer timescales of a few months to half a year, Saturn’s moons produce 0.5 km oscillations in the  $z_{max}$  of the moon. On decade timescales,  $\langle z_{max} \rangle$ , the median height of the moon above the ring plane is roughly constant. Thus, stirring by Saturn’s moons appears capable of maintaining the large inclination of Daphnis relative to the A ring.

The predicted oscillations of Daphnis are sensitive to several characteristics of our calculations. In our approach to ring dynamics, ring particles have no self gravity and therefore do not react to changes in local surface density. Furthermore, the ring plane itself is fixed and does not evolve in response to torques. Despite these limitations, the calculations make a robust prediction: as the mass of a small moon grows and as the surface density of ring particles around the satellite declines, the distant moons of Saturn produce an oscillatory behavior in the height of the small moon above the ring plane. These oscillations can prevent small moons like Daphnis from migrating through the ring.

The predicted quasi-periodic oscillations in the altitude of Daphnis above the ring plane are detectable. The predicted amplitude of 200–400 m is a significant fraction of the typical maximum altitude of roughly 9 km. The quasi-period of a few months yields a rate  $\dot{z}_{max} \approx 0.4\text{--}0.8 \text{ km yr}^{-1}$ , a few times larger than the rates of motion derived for the propeller moon Blériot (Tiscareno et al. 2010). Thus, accurate observations of Daphnis’ inclination or maximum height above the ring plane would test our interpretation.

### 5.3. Summary

Our results suggest several plausible origins for Daphnis. A ‘young’ Daphnis can result from an impact fragment or from growth beyond the outer edge of the A ring. In both of these recent origin scenarios, ring material on either side of the Keeler gap should damp Daphnis’ orbit on short,  $\sim 1000 \text{ yr}$ , timescales. Interactions between Daphnis and the rings should also induce fast migration.

An ‘old’ Daphnis has been resident in the rings for timescales exceeding  $\sim 10,000 \text{ yr}$ . Because



external processes prevent Daphnis from migrating, Daphnis’ residence time in the ring could approach the ring lifetime of  $\gtrsim 0.1\text{--}1$  Gyr. Our simulations show that orbital resonances with distant moons can impact Daphnis’ orbit. Identifying the combination of physical properties for Daphnis, the rings, and the distant moons needed to maintain Daphnis in its current orbit requires a comprehensive suite of simulations that is beyond the scope of this paper.

Our simulations also demonstrate that orbital interactions between Daphnis and distant moons (e.g., Mimas and Tethys) outside of any resonance can impact Daphnis’ orbit. Maintaining Daphnis in its current orbit requires a fine balance between stirring by the distant moon(s) and damping by ring particles outside the Keeler gap.

#### 5.4. Observational Tests

Observations can test all of these scenarios. If Daphnis is young, we predict detectable, monotonic changes in the orbital parameters  $(a, e, i)$ . If Daphnis is old, changes in  $(a, e, i)$  depend on the importance of resonances. Outside resonance, we expect modest changes in phase with the motions of distant moons such as Mimas. Within resonance, the behavior depends on the strength of the resonance relative to damping by the ring. Although measuring orbital parameters in a chaotic reference frame is challenging, direct measurement of Daphnis’ altitude above the ring plane and position in the Keeler gap provide equivalent tests of our predictions.

### 6. Conclusions

Saturn’s A ring is rich in structure, with an amazing, complex variety of transient and long-lived features (e.g., Esposito 2010). The smallest ring particles lie in a matrix of self-gravity wakes, which form coherent features on scales smaller than 100 m (Hedman et al. 2007). The 150 or so moonlets embedded in the ring have physical radii between 50 m and 250 m, and are located in three  $\sim 1000$  km annuli (Tiscareno et al. 2008). The small moons Pan and Daphnis orbit within distinct gaps with very low surface density. Together, these moons, moonlets, and smaller particles provide an excellent testbed for migration theory (see also Crida et al. 2010; Pan & Chiang 2010; Rein & Papaloizou 2010; Salmon & Charnoz 2010; Tiscareno 2012, and references therein).

As outlined in Figures 1 and 2, theory predicts several distinct modes of migration through the rings. In the very viscous A ring, moonlets with  $r_H \lesssim 0.1$  km migrate on timescales much longer than the age of the solar system. Large moons with  $r_H \gtrsim 20\text{--}30$  km also migrate very slowly. Between these limits, migration timescales are shorter than the ring lifetime. For  $r_H \approx 2\text{--}20$  km, the timescales are comparable to a human lifetime.

In our simulations of Saturn’s A ring, fast migration of small moons with  $r_H \approx 2\text{--}20$  km is ubiquitous. When a small moon lies within a gap, it eventually pulls enough material from the gap edges to begin fast migration (Figs. 3–4). When a small moon is embedded within a continuous ring, it eventually clears enough material from its corotation zone to begin fast migration (Fig. 5).

In a pristine ring of small particles, numerical simulations show that moonlets and small moons

migrate at the rates predicted by analytic theory (Figs. 8 and 9). In numerical simulations that include damping, gravitational interactions between small moons and ring particles, and viscous spreading, the moons clear their corotation zones on timescales  $T_{\text{clear}}$ . When the viscous timescale is longer than  $T_{\text{clear}}$ , these moons open a gap in the ring and begin to migrate. As long as  $r_{\text{H}} \lesssim r_{\text{fast}}$ , migration is fast. Otherwise, migration is slow.

In Saturn’s rings, damping and viscous spreading smooth out the wakes left behind by migrating moons. Thus, multiple moons can easily migrate rapidly through the rings. This situation contrasts with protoplanetary disks, where stirring by migrating protoplanets overcomes damping by smaller planetesimals (Bromley & Kenyon 2011b).

Several physical processes within the rings limit or halt migration. Interactions between small moons and (i) very large ring particles or (ii) local enhancements in ring surface density lead to stochastic migration, often reducing migration rates significantly (Crida et al. 2010; Rein & Papaloizou 2010; Tiscareno 2012). Migrating moonlets and very small moons cannot pass the ‘resonant barriers’ formed by moons outside the A ring (§4.4). Pairs of resonances can ‘corral’ these objects and prevent them from migrating in or out through the ring (Fig. 10). Stirring by distant moons outside resonance can also overcome damping and prevent migration (§4.5).

These results lead to several clear conclusions regarding migration in the A ring.

- **Propeller moonlet migration.** With Hill radii less than  $r_{\text{gap}} \approx 2$  km (Tiscareno et al. 2008), the propeller moonlets should experience slow, embedded migration with radial drift rates below  $10 \text{ m yr}^{-1}$  (Fig. 2). Stochastic migration in a self-gravitating ring (Rein & Papaloizou 2010; Crida et al. 2010), interactions with surface density variations in the ring (Tiscareno 2012), and oscillatory motion from interactions with corotating material (Pan & Chiang 2010, 2012) have similar low drift rates. For most moonlets, measurements of radial drift limit the rate to below  $0.1 \text{ km yr}^{-1}$ . At least one larger moonlet, Blériot, shows non-Keplerian motion (Tiscareno et al. 2010), with a drift rate that varies in time. Our new results suggest that the radial drift of Blériot and other moonlets can be confined by orbital resonances. Indeed, most propellers appear to be confined to the ‘corral’ between the Mimas 5:3 resonance and the Janus/Epimetheus 5:4 resonance (Fig. 10).
- **The propeller moonlet size distribution.** Moonlets have a range of sizes up to about  $r_{\text{H}} \sim 1.5$  km (Tiscareno et al. 2008, 2010). Migration theory predicts an upper limit of  $r_{\text{gap}} \approx 2$  km. Larger objects migrate out of the ring on timescales of 100–1000 yr. The good agreement between  $r_{\text{gap}}$  and the maximum size of propellers is a strong confirmation of migration theory.
- **Non-Keplerian motion of moonlets.** Moonlets orbit Saturn in a gravitational field which is constantly modified by much more massive moons orbiting at larger distance. The constant jostling of moonlets by distant moons results in chaotic radial variations in distance from Saturn (Fig. 9). Aside from complicating the measurement of a moonlet’s orbital elements within our simulations, this motion may complicate interpretations of non-Keplerian motion of moonlets within the ring (e.g., Blériot, Tiscareno et al. 2010).

- **The ‘young’ Daphnis.** If some external physical mechanism cannot maintain Daphnis in its current orbit, it must be a recent,  $\sim 10^3 - 10^4$  yr, addition to the ring. Migration theory predicts rapid damping in  $(e, i)$  followed by fast migration. Instruments on board *Cassini* can measure the predicted damping in height above the ring plane.
- **The ‘old’ Daphnis.** If orbital resonances or stirring by distant moons can maintain Daphnis in its current orbit, it may be very old. From our simulations, we identify sources of stirring which might maintain Daphnis’ orbit for timescales exceeding  $10^4$  yr. Measuring oscillations in  $(a, e, i)$  can place strong constraints on this mechanism.
- **Pan.** With  $r_H = 19$  km at an orbital distance of 133,584 km, this small moon orbits within the 300 km-wide Encke gap (Cuzzi & Scargle 1985; Jacobson et al. 2008). Pan’s Hill radius is very close to  $r_{\text{fast}}$ . As with Daphnis, orbital resonances and stirring from distant moons probably prevent any form of migration. In addition, these effects may operate to help maintain the Encke gap, whose edges are relatively far,  $\sim 8r_H$ , from Pan. The torques from ring material in this configuration are too weak to cause measurable radial drift.
- **Atlas.** Orbiting within the Roche Division at the outer edge of the A ring, Atlas’ Hill radius,  $r_H = 22$  km, is also close to  $r_{\text{fast}}$ . Although it is too far away from ring material to have any chance at migrating, Atlas may have migrated out through the ring to its present location. As with Pan and Daphnis, understanding the internal physics of ring material and the interactions with distant moons might yield clues about its origin and recent history.
- **Pan and Atlas.** For both moons, detecting or limiting variations in  $(a, e, i)$  can provide important constraints on the physical mechanisms within the ring and interactions between ring particles, these small moons, and distant moons.

To conclude, our analytic estimates and numerical simulations demonstrate that Saturn’s rings are an important laboratory for testing migration theory. Current results are encouraging. Within the A ring, we can explain aspects of the radial and size distributions of propellers and we identify plausible mechanisms for limiting migration in Daphnis. We also identify several important observational tests which can be accomplished with current satellites.

Aside from including additional constraints on ring properties as new observations provide them, future studies of ring dynamics will eventually require including the ring self-gravity directly. Self-gravity adds to the rich dynamical structure of the rings (e.g., Lewis & Stewart 2009), which likely has interesting consequences for the migration of moons and moonlets (e.g., Fig. 9).

We are grateful for advice and comments from M. Geller. We thank A. Youdin for suggesting important improvements to the manuscript. Numerous helpful comments from the referee, M. Tiscareno, significantly improved the text. Portions of this project were supported by *NASA’s Astrophysics Theory Program* and the *Origin of Solar Systems Program* through grant NNX10AF35G and the *Outer Planets Program* through grant NNX11AM37G. We also acknowledge generous allotments of computer time on the NASA ‘discover’ computer cluster operated by the National Center for Climate Simulation.

## Appendix

The onset of fast migration relies on the presence of some ring material within  $\sim 4r_{\text{H}}$  of a small moon. For a moon within a gap, fast migration proceeds only when the half-width of the gap is  $\lesssim 4r_{\text{H}}$ . Because the relationship between the moon and the size of the gap it creates is critical to migration, we consider several approaches to assess this relationship.

In the torque-balance approach (e.g., Lissauer et al. 1981), the viscous torque on ring material as it diffuses into a gap of width  $\Delta a$  is set equal to the torque at the gap edge applied by the satellite. From weak-scattering theory (Lin & Papaloizou 1979), this balance yields a simple relationship between the gap half-width and the satellite’s Hill radius:

$$\Delta a \sim 2 \left( \frac{GM}{a^5 \nu^2} \right)^{1/6} r_{\text{H}}^2. \quad (1)$$

If the time to fill the gap is the viscous time (e.g.,  $T_{\text{fill}}$  in eq. [7] in the main text), it is possible to eliminate the viscosity in this expression and derive a minimum gap size, as in eq. (2) for  $r_{\text{gap}}$ .

An alternative approach equates the radial distance ring material can diffuse in a synodic period,  $\sqrt{\nu T_{\text{syn}}}$ , with the displacement in semimajor axis a particle receives after every close encounter with the satellite (proportional to the right-hand-side of eq. (1) above; see also eq. [5] of Bromley & Kenyon 2011b). This balanced is achieved at an orbital distance from the satellite

$$\Delta a \sim \left( \frac{GM}{a^5 \nu^2} \right)^{1/18} r_{\text{H}}^{4/3}. \quad (2)$$

This result is similar to the result in eq. (1).

More detailed treatments derive some form of the radial diffusion equation across the gap and solve explicitly for the surface density distribution and the half-width of the gap (e.g., Hourigan & Ward 1984; Rafikov 2001). Although these solutions yield much better estimates for the surface density distribution, results for the half-width of the gap differ from the simpler treatments by less than a factor of two. Given the uncertainties, either eq. (1) or eq. (2) provides a reasonable approximation to the half-width.

To apply these two results to Saturn’s A ring, we adopt the nominal parameters in eqs. (14)–(16) from the main text and derive

$$\Delta a \sim 0.97 \left[ \frac{r_{\text{H}}}{1 \text{ km}} \right]^2 \left[ \frac{85 \text{ cm}^2/\text{s}}{\nu_{\text{rad}}} \right]^{1/3} \left[ \frac{1.3 \times 10^5 \text{ km}}{a} \right]^{5/6} \text{ km} \quad (3)$$

for balancing the torques and

$$\Delta a \sim 1.4 \left[ \frac{r_{\text{H}}}{1 \text{ km}} \right]^{4/3} \left[ \frac{85 \text{ cm}^2/\text{s}}{\nu_{\text{rad}}} \right]^{1/9} \left[ \frac{1.3 \times 10^5 \text{ km}}{a} \right]^{5/18} \text{ km} \quad (4)$$

for balancing scattering and viscous diffusion. For small moons capable of fast migration,  $r_{\text{H}} \approx 2\text{--}5$  km, these approaches yield similar results for  $\Delta a$ . For much larger moons, torque balance consistently yields a larger half-width.

For the rest of this section, we focus on half-widths derived by balancing scattering and viscous diffusion. Requiring  $\Delta a \gtrsim 4r_H$  yields the maximum Hill radius for a satellite capable of drawing material from the gap edges,  $\sim 23$  km, when scattering balances viscous diffusion. This limit is comparable to  $r_{\text{fast}}$ .

In principle, moons with  $r_H \gtrsim 23$  km can prevent material from encroaching within  $4r_H$ . These moons migrate slowly in the type II mode. Because gravitational scattering falls off so steeply with orbital distance from the satellite, viscous diffusion constantly tries to drive material into the gap. If diffusion produces a higher surface density and viscosity at the edges of a gap, the gap will shrink, enabling the satellite to draw material away from the gap, possibly initiating fast migration.

To compare the simple theory with Daphnis in the Keeler Gap and Pan in the Encke Gap, we adopt  $r_H \approx 5$  km for Daphnis and  $r_H \sim 20$  km for Pan. For Daphnis, the balance between scattering and viscous diffusion occurs at  $\Delta a \sim 12$  km, somewhat smaller than the observed half width,  $\sim 13$ – $20$  km, of the Keeler gap (Weiss et al. 2009). For Pan, the balance is at  $\Delta a \sim 75$  km, much smaller than the observed half-width,  $\sim 160$  km, of the Encke Gap. Based on this analysis, we identify Daphnis as a good candidate for fast migration. Pan is a poor candidate for fast migration, at least under current conditions in the Encke Gap. However, barring other effects such as resonances with distant moons, Pan may be unable to halt long-term diffusion of ring material to within  $4r_H$ .

In our calculations, large moons achieve a balance between viscous diffusion and gravitational scattering. The numerical results support the limits derived in eq. (4). Moons with  $r_H \gtrsim 20$ – $25$  km can migrate in the type II mode. Smaller moons with  $r_H \approx 2$ – $20$  km may undergo fast migration.

## REFERENCES

- Alexander, R. D., & Armitage, P. J. 2009, *ApJ*, 704, 989
- Allen, R. R. 1969, *AJ*, 74, 497
- Artymowicz, P. 2004, *Debris Disks and the Formation of Planets*, 324, 39
- Borderies, N., Goldreich, P., & Tremaine, S. 1984, *ApJ*, 284, 429
- Bromley, B., & Kenyon, S. J. 2006, *AJ*, 131, 2737
- Bromley, B., & Kenyon, S. J., 2011, *ApJ*, 731, 101
- Bromley, B., & Kenyon, S. J., 2011, *ApJ*, 735, 29
- Bryden, G., Chen, X., Lin, D. N. C., Nelson, R. P., & Papaloizou, J. C. B. 1999, *ApJ*, 514, 344
- Champanois, S., & Vienne, A. 1999, *Celestial Mechanics and Dynamical Astronomy*, 74, 111
- Champanois, S., & Vienne, A. 1999, *Icarus*, 140, 106
- Cook, A. F., & Franklin, F. A. 1964, *AJ*, 69, 173
- Charnoz, S., Salmon, J., & Crida, A. 2010, *Nature*, 465, 752

- Charnoz, S., Crida, A., Castillo-Rogez, J. C., et al. 2011, *Icarus*, 216, 535
- Colwell, J. E., Nicholson, P. D., Tiscareno, M. S., et al. 2009, *Saturn from Cassini-Huygens*, 375
- Crida, A., Morbidelli, A., & Masset, F. 2006, *Icarus*, 181, 587
- Crida, A., Papaloizou, J. C. B., Rein, H., Charnoz, S., & Salmon, J. 2010, *AJ*, 140, 944
- Cuzzi, J. N., Lissauer, J. J., & Shu, F. H. 1981, *Nature*, 292, 703
- Cuzzi, J., Clark, R., Filacchione, G., et al. 2009, *Saturn from Cassini-Huygens*, 459
- Cuzzi, J. N., Burns, J. A., Charnoz, S., et al. 2010, *Science*, 327, 1470
- Cuzzi, J. N., & Durisen, R. H. 1990, *Icarus*, 84, 467
- Cuzzi, J. N., & Scargle, J. D. 1985, *ApJ*, 292, 276
- D’Angelo, G., Dapnis, R. H., & Lissauer, J. J. 2010, arXiv:1006.5486
- D’Angelo, G., Kley, W., & Henning, T. 2003, *ApJ*, 586, 540
- D’Angelo, G., & Marzari, F. 2012, *ApJ*, 757, 50
- Esposito, L. W. 2010, *Annual Review of Earth and Planetary Sciences*, 38, 383
- Gladman, B. 1993, *Icarus*, 106, 247
- Giorgini, J. D., Yeomans, D. K., Chamberlin, A. B., et al. 1996, *Bulletin of the American Astronomical Society*, 28, 1158
- Goldreich, P., & Tremaine, S. D. 1978, *Icarus*, 34, 227
- Goldreich, P., & Tremaine, S. D. 1978, *Icarus*, 34, 240
- Goldreich, P., & Tremaine, S. 1979, *ApJ*, 233, 857
- Goldreich, P., & Tremaine, S. 1980, *ApJ*, 241, 425
- Goldreich, P., & Tremaine, S. 1981, *ApJ*, 243, 1062
- Goldreich, P., & Tremaine, S. 1982, *ARA&A*, 20, 249
- Hahn, J. M. 2007, *ApJ*, 665, 856
- Hahn, J. M. 2008, *ApJ*, 680, 1569
- Hahn, J. M., & Malhotra, R. 1999, *AJ*, 117, 3041
- Hahn, J. M., Spitale, J. N., & Porco, C. C. 2009, *ApJ*, 699, 686
- Hedman, M. M., Nicholson, P. D., Salo, H., et al. 2007, *AJ*, 133, 2624
- Hourigan, K., & Ward, W. R. 1984, *Icarus*, 60, 29

- Ida, S., Bryden, G., Lin, D. N. C., & Tanaka, H. 2000, *ApJ*, 534, 428
- Jacobson, R. A., Antreasian, P. G., Bordi, J. J., et al. 2006, *AJ*, 132, 2520
- Jacobson, R. A., Spitale, J., Porco, C. C., et al. 2008, *AJ*, 135, 261
- Kenyon, S. J., & Bromley, B. C. 2004, *AJ*, 127, 513
- Kenyon, S. J., & Bromley, B. C. 2008, *ApJS*, 179, 451
- Kenyon, S. J., & Bromley, B. C. 2009, *ApJ*, 690, L140
- Kirsh, D. R., Duncan, M., Brasser, R., & Levison, H. F. 2009, *Icarus*, 199, 197
- Levison, H. F., Morbidelli, A., Gomes, R., & Backman, D. 2007, *Protostars and Planets V*, 669
- Lewis, M. C., & Stewart, G. R. 2000, *AJ*, 120, 3295
- Lewis, M. C., & Stewart, G. R. 2009, *Icarus*, 199, 387
- Lewis, M., Stewart, G., Leezer, J., & West, A. 2011, *Icarus*, 213, 201
- Lin, D. N. C., & Papaloizou, J. 1979, *MNRAS*, 186, 799
- Lin, D. N. C., & Papaloizou, J. 1986, *ApJ*, 309, 846
- Lissauer, J. J., & Cuzzi, J. N. 1982, *AJ*, 87, 1051
- Lissauer, J. J., Shu, F. H., & Cuzzi, J. N. 1981, *Nature*, 292, 707
- Lissauer, J. J., Fabrycky, D. C., Ford, E. B., et al. 2011, *Nature*, 470, 53
- Lissauer, J. J., Goldreich, P., & Tremaine, S. 1985, *Icarus*, 64, 425
- Lubow, S. H., & Ida, S. 2010, *arXiv:1004.4137*
- Malhotra, R. 1993, *Nature*, 365, 819
- Masset, F. S., & Papaloizou, J. C. B. 2003, *ApJ*, 588, 494
- Masset, F., & Snellgrove, M. 2001, *MNRAS*, 320, L55
- Morbidelli, A., & Crida, A. 2007, *Icarus*, 191, 158
- Morbidelli, A., Tsiganis, K., Crida, A., Levison, H. F., & Gomes, R. 2007, *AJ*, 134, 1790
- Ohtsuki, K. 1992, *Icarus*, 98, 20
- Paardekooper, S.-J., Baruteau, C., Crida, A., & Kley, W. 2010, *MNRAS*, 401, 1950
- Paardekooper, S.-J., Baruteau, C., & Kley, W. 2011, *MNRAS*, 410, 293
- Pan, M., & Chiang, E. 2010, *ApJ*, 722, L178
- Pan, M., & Chiang, E. 2012, *AJ*, 143, 9

- Pan, M., Rein, H., Chiang, E., & Evans, S. N. 2012, MNRAS, in press (arXiv:1206.3583)
- Papaloizou, J. C. B., Nelson, R. P., Kley, W., Masset, F. S., & Artymowicz, P. 2007, *Protostars and Planets V*, 655
- Perrine, R. P., Richardson, D. C., & Scheeres, D. J. 2011, *Icarus*, 212, 719
- Porco, C. C., and the Cassini Imaging Team, 2005, *IAU Circ.*, 8524, 1
- Porco, C. C., Weiss, J. W., Richardson, D. C., et al. 2008, *AJ*, 136, 2172
- Pringle, J. E. 1981, *ARA&A*, 19, 137
- Rafikov, R. R. 2001, *AJ*, 122, 2713
- Rein, H., & Papaloizou, J. C. B. 2010, *A&A*, 524, A22
- Salmon, J., & Charnoz, S. 2010, *Bulletin of the American Astronomical Society*, 42, 981
- Salmon, J., Charnoz, S., Crida, A., & Brahic, A. 2010, *Icarus*, 209, 771
- Salo, H., & Karjalainen, R. 2003, *Icarus*, 164, 428
- Salo, H., & Schmidt, J. 2010, *Icarus*, 206, 390
- Shakura, N. I., & Sunyaev, R. A. 1973, *A&A*, 24, 337
- Showalter, M. R. 1991, *Nature*, 351, 709
- Showalter, M. R., Cuzzi, J. N., Marouf, E. A., & Esposito, L. W. 1986, *Icarus*, 66, 297
- Shu, F. H., Cuzzi, J. N., & Lissauer, J. J. 1983, *Icarus*, 53, 185
- Syer, D., & Clarke, C. J. 1995, *MNRAS*, 277, 758
- Tanaka, H., Takeuchi, T., & Ward, W. R. 2002, *ApJ*, 565, 1257
- Thomas, P. C. 2010, *Icarus*, 208, 395
- Tiscareno, M. S., Burns, J. A., Nicholson, P. D., Hedman, M. M., & Porco, C. C. 2007, *Icarus*, 189, 14
- Tiscareno, M. S., Burns, J. A., Hedman, M. M., et al. 2006, *Nature*, 440, 648
- Tiscareno, M. S., Burns, J. A., Hedman, M. M., & Porco, C. C. 2008, *AJ*, 135, 1083
- Tiscareno, M. S., Burns, J. A., Sremčević, M., et al. 2010, *ApJ*, 718, L92
- Tiscareno, M. S. 2012, *Planetary and Space Science*, in press (arXiv:1206.4942).
- Tiscareno, M. S. 2013, in *Planets, Stars, and Stellar Systems, Volume 3: Solar and Stellar Systems* Oswald TD, French L, and Kalas P, eds. (Dordrecht: Springer), in press (arXiv:1112.3305).
- Vienne, A., & Duriez, L. 1992, *A&A*, 257, 331



Ward, W. R. 1988, *Icarus*, 73, 330

Ward, W. R. 1997, *Icarus*, 126, 261

Ward, W. R., & Hourigan, K. 1989, *ApJ*, 347, 490

Weidenschilling, S. J. 1989, *Icarus*, 80, 179

Weiss, J. W., Porco, C. C., & Tiscareno, M. S. 2009, *AJ*, 138, 272

Youdin, A. N., & Kenyon, S. J. 2012, arXiv:1206.0738

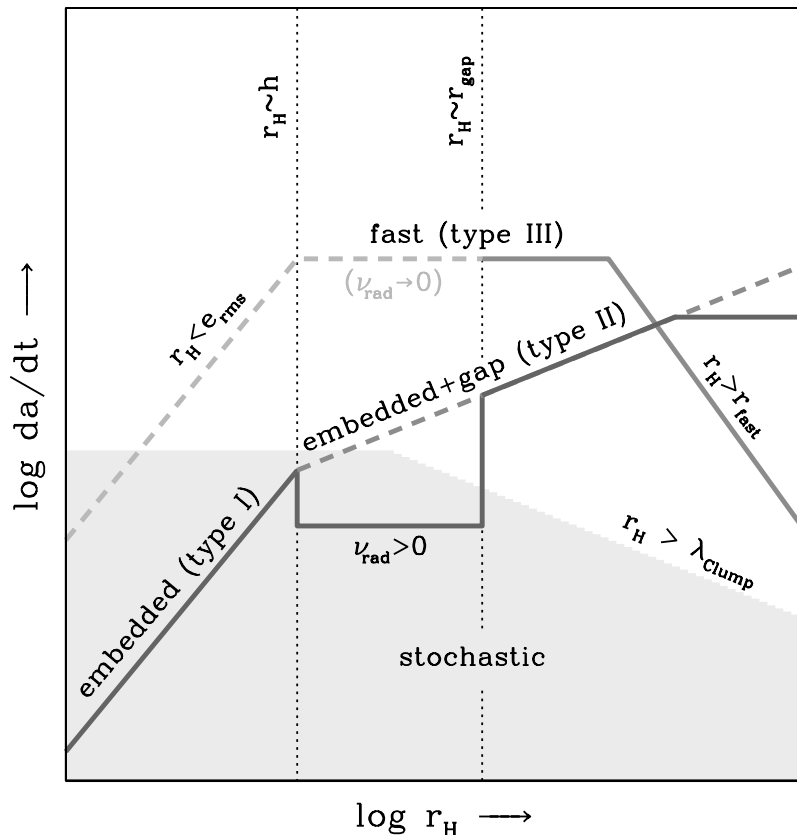


Fig. 1.— A qualitative comparison of predicted migration rates as a function of Hill radius for satellites in a particle disk. The solid curves show rates in viscous disks; the dashed curves apply in the limit of zero viscosity where  $r_{\text{gap}}$  — the Hill radius of a satellite that can clear a gap — is set by the disk scale height,  $h$ . A satellite drifts radially according to the larger of the fast and embedded migration rates for its Hill radius. The dip in the embedded migration rate for  $\nu_{\text{rad}} > 0$  illustrates that migration may be suppressed in a viscous disk if  $r_H$  is in the “transgap” regime, where the satellite is larger than the disk scale height but not large enough to open a gap. The curve representing fast migration shows an upper plateau with a migration rate independent of  $r_H$ , a steep decline above the limiting Hill radius  $r_{\text{fast}}$  (see text), and a similarly sharp attenuation in  $da/dt$  below  $r_H = h$ , where the typical disk particle eccentricity  $e_{\text{rms}}$  becomes important. The shaded region is suggestive of radial drifts from stochastic migration within some fixed time period. If the source of the stochasticity is clumping of disk particles on scales of  $\lambda_{\text{clump}}$ , then the effective rate falls off as  $1/r_H$ . Otherwise the effective rate is constant.

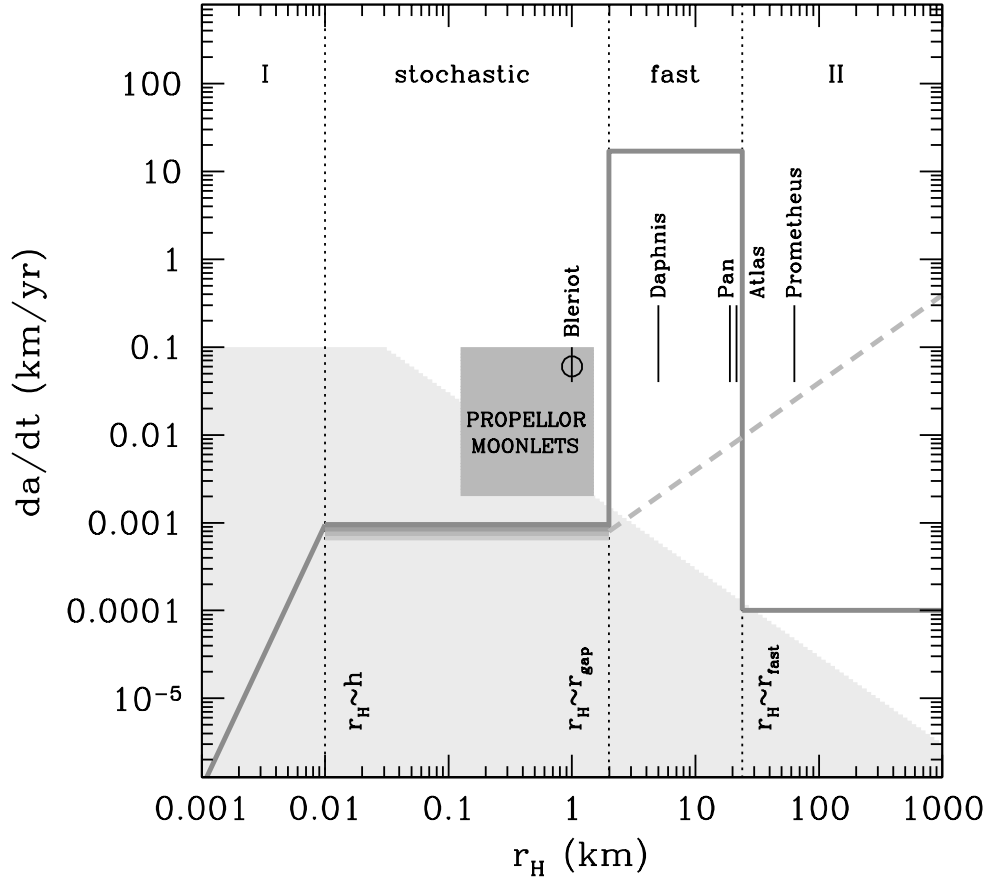


Fig. 2.— A schematic of predicted migration rates as a function of Hill radius for satellites in Saturn’s A ring. The solid curve shows the upper limit of the predicted rate for a wide range of satellite masses. The dashed line is the low-viscosity limit of embedded migration. For  $r_H \gtrsim r_{\text{fast}}$ , the solid line below the dashed line reflects the viscosity-dominated Type II mode. The shaded region represents stochastic migration, bounded by an approximate average yearly radial drift assuming that the ring contains clumps of 30 m (these rates are drawn from a broad range reported by Crida et al. (2010) and Rein & Papaloizou (2010)). The data points and shaded region for the propeller moonlets indicate Hill radii only; with the exception of the moonlet Blériot, migration has not been detected.

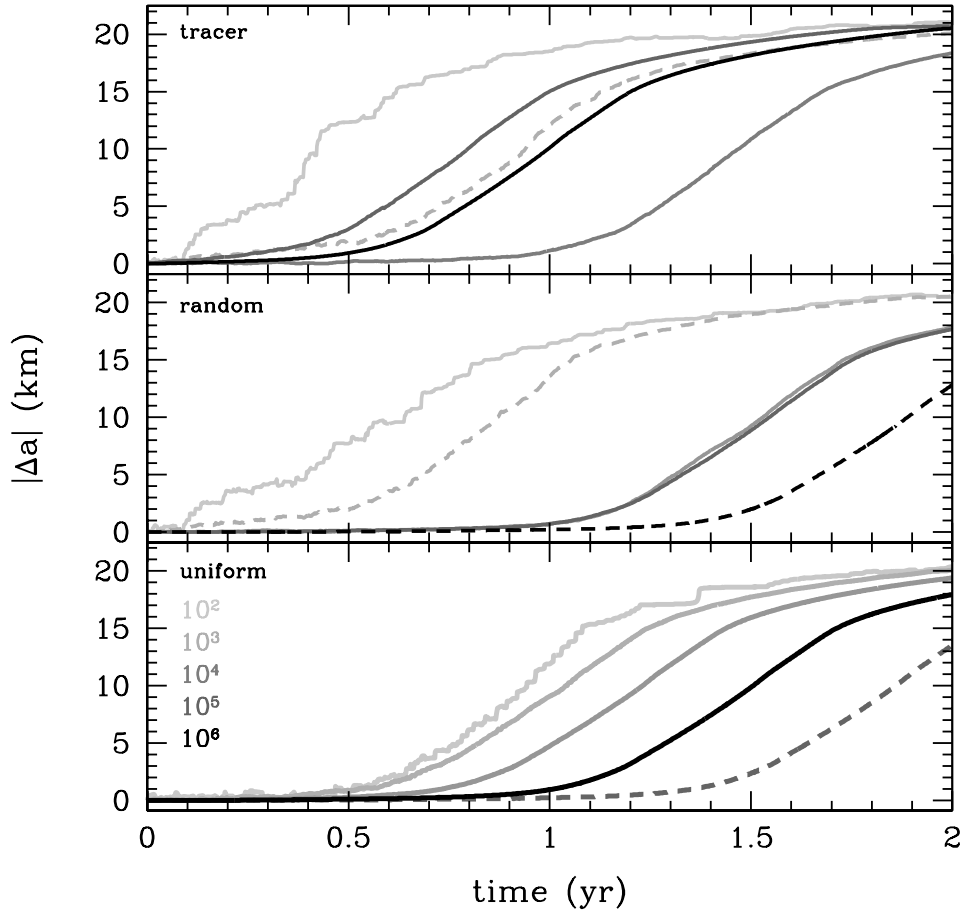


Fig. 3.— Fast migration of small moons in a ring of massive particles with  $\Sigma = 40 \text{ g/cm}^2$ , a total annular width of 56 km, and a gap with a halfwidth of 14 km, which covers the corotation zone. Simulations begin with the moon precisely centered in the gap. Each curve represents the change in orbital distance,  $\Delta a$ , of a moon with  $r_{\text{H}} = 7 \text{ km}$  and an initial semimajor axis of 130,000 km. In each simulation, the particles in the ring have identical mass, set to  $10^{-2}$  (lightest shading),  $10^{-3}$ ,  $10^{-4}$ ,  $10^{-5}$ , or  $10^{-6}$  (darkest shading) times the mass of the moon. Solid (dashed) lines indicate inward (outward) migration. Although migration is more stochastic with larger ring particles, the migration rate is nearly independent of the masses of ring particles. When a moon reaches the edge of the ring, migration ceases.

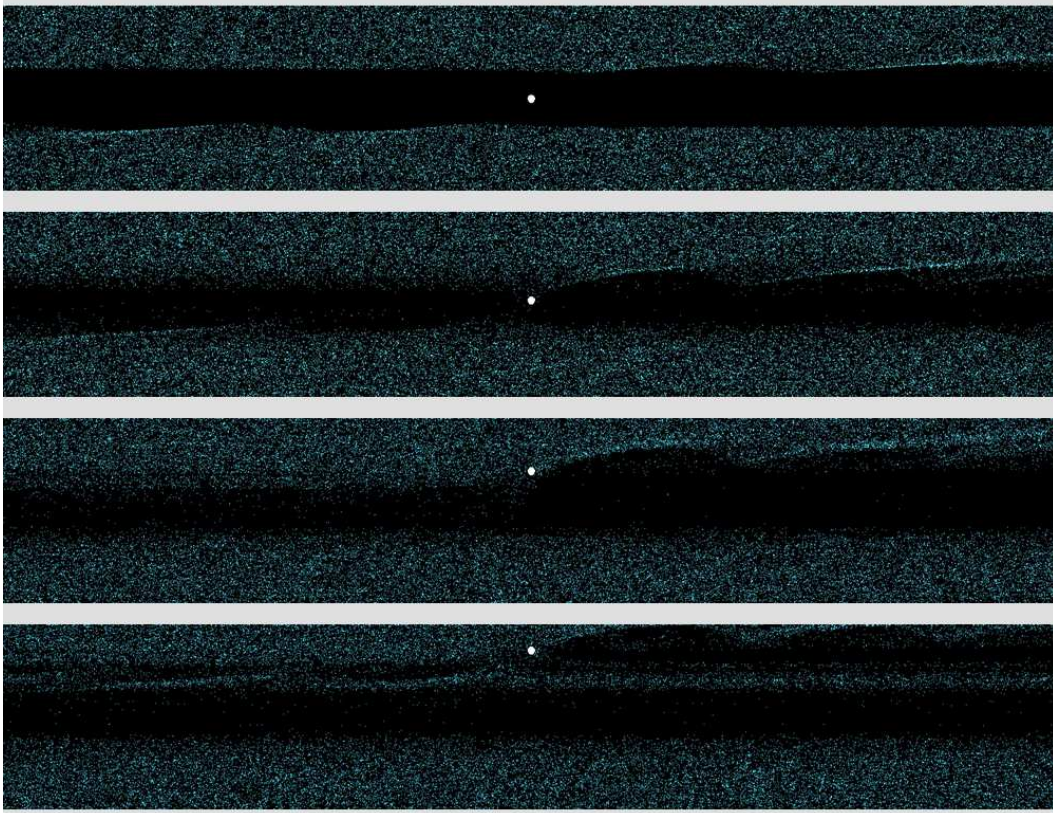


Fig. 4.— Snapshots of small moon migration in a closing gap. The top image shows the location of a Daphnis-size moon ( $r_H = 4.9$  km, the central white disk of 2.3 km in radius, the approximate physical size of Daphnis) at Daphnis’s orbital distance (136,505 km) when it is initially on a circular orbit in a pristine ring with uniform surface density  $\Sigma = 40$  g/cm<sup>2</sup>, centered on a clear annulus the size of the Keeler gap (full width of 40 km). The ring particles (masses equal to 0.1% times that of the satellite) are indicated with a brightness that correlates with density. The lower three images show views from the same orbital distance from Saturn but at times equal to 46.6 yr (second from top), 48.2 yr, and 49 yr. Radial diffusion ( $\nu_{\text{rad}} = 85$  cm<sup>2</sup>/s) causes ‘the ring to slowly creep into the gap, but once particles get close, fast migration initiates and the moon heads toward Saturn. Each image represents an area of 800 km in width and 120 km in height, oriented so that Saturn is located toward the top of the page. The “exposure time” for each image is several orbital periods, to enhance the structures in the ring.

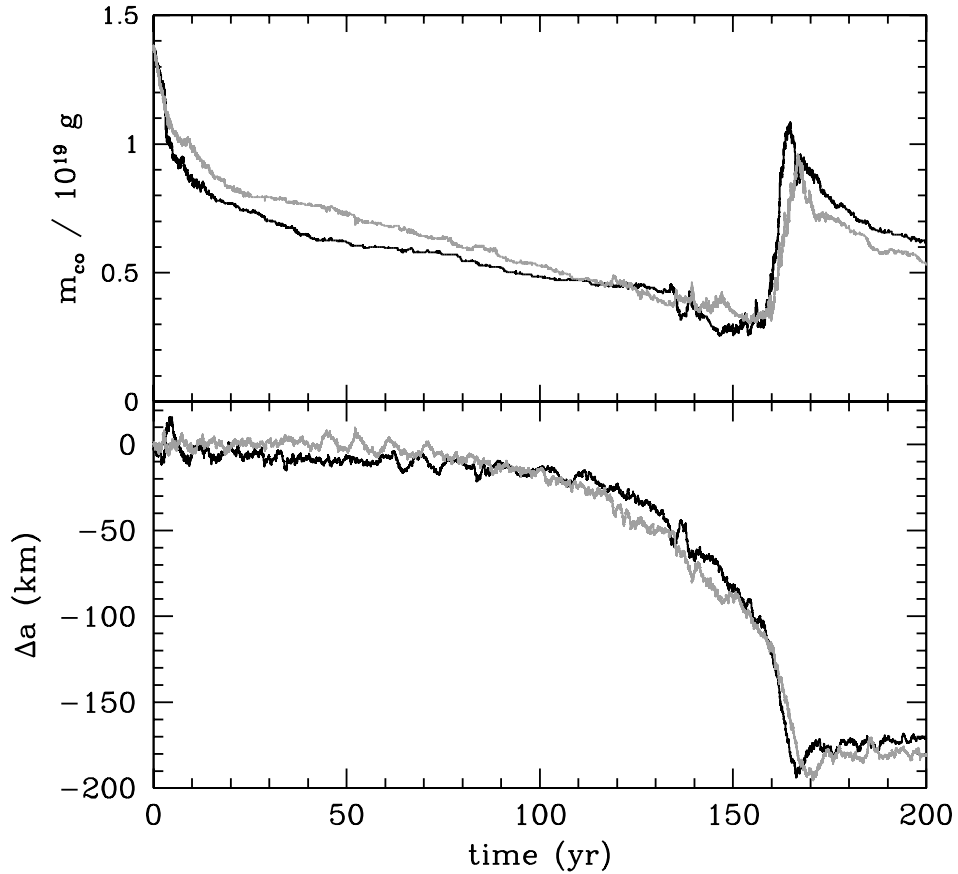


Fig. 5.— The disk mass in the corotation zone and the radial drift of a small moon with  $r_H = 14$  km. The starting orbital distance is 130,000 km. The upper plot shows the instantaneous disk mass  $m_{\text{co}}$  inside an annulus of half-width  $2r_H$ ; the lower plot is the orbital distance of the moon relative to its starting position. The black curve refers to calculations for the moon and ring alone; the light curve indicates results for calculations which include Saturn’s prominent moons (Fig. 10). In both instances, migration stops after  $\sim 170$  years, when the moon hits the inner edge of the simulated disk.

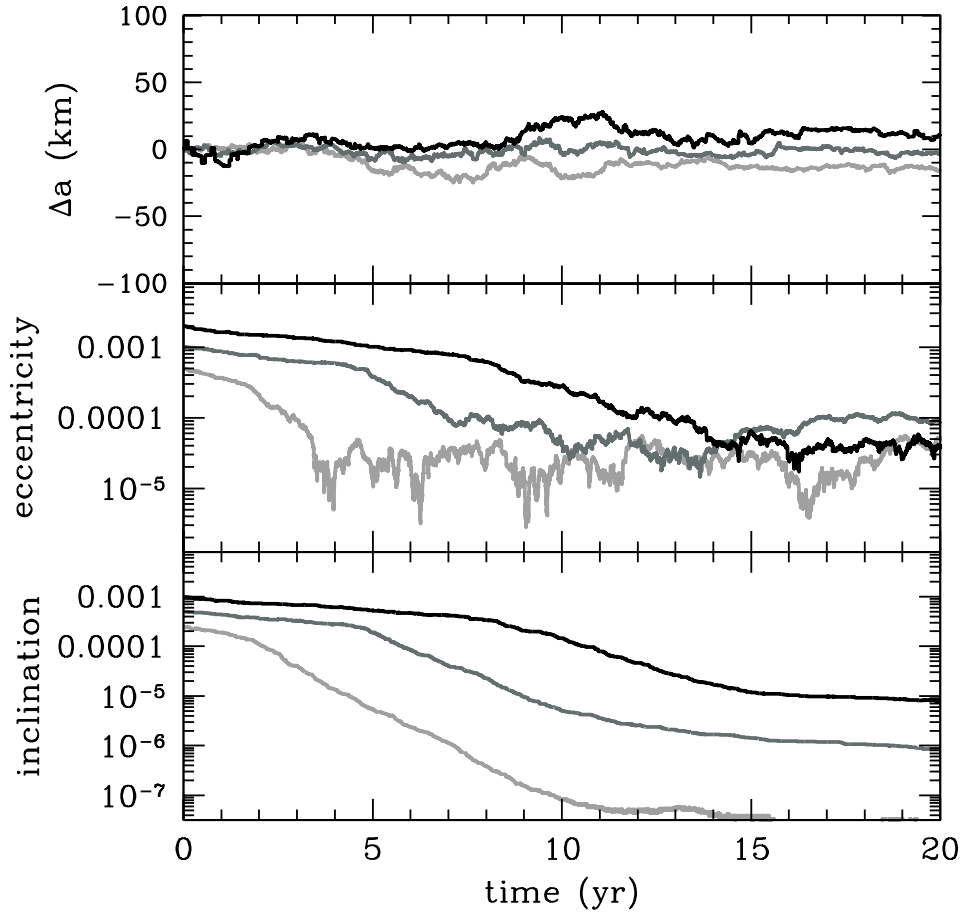


Fig. 6.— Orbital settling of captured small moons. Simulations of moons with Hill radii of 10 km (light gray curves), 14 km (dark gray curves), and 18 km (black curves) show the evolution of orbital elements in an initially uniform disk with A ring parameters. In all cases, the time for each moon to become embedded in the disk is very short.

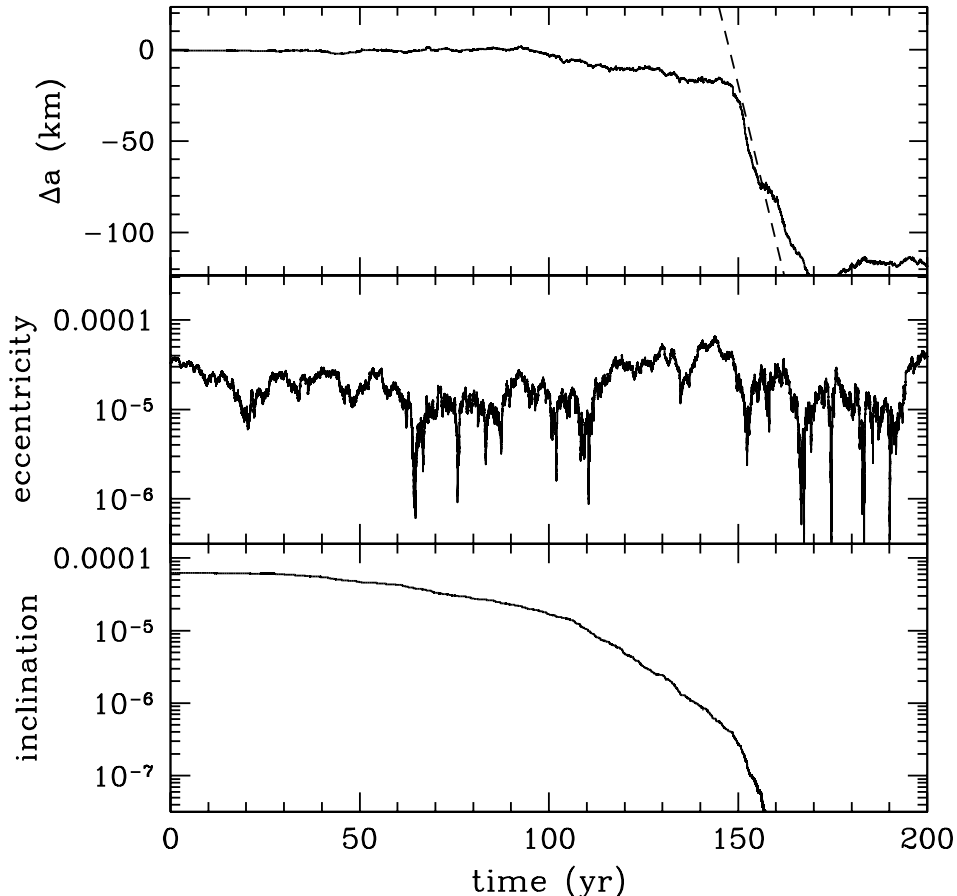


Fig. 7.— The onset of fast migration of a captured moon. The traces show the change in semimajor axis (upper plot), eccentricity (middle plot) and inclination (lower plot) of a small moon with  $r_{\text{H}} = 6.5$  km in a disk with  $\Sigma = 20$  g/cm<sup>3</sup>. The initial orbit of the moon is the same as for Daphnis; the disk properties are modified for computational feasibility. The disk has an 80 km-wide gap (similar to the Keeler gap along Daphnis’ orbit in terms of the moon’s Hill radii). The disk particles’ eccentricity and inclination damp as expected for the A ring. The viscosity, however, is turned up by a factor of 15, thus reducing the viscous spreading time in the gap by a factor of 3 compared to the Keeler gap. The simulation shows that the eccentricity damps quickly, but migration does not begin until the inclination is also small. After migration starts, its rate is comparable to the theoretical prediction (dashed curve), and it halts once the moon nears the edge of the simulated disk.



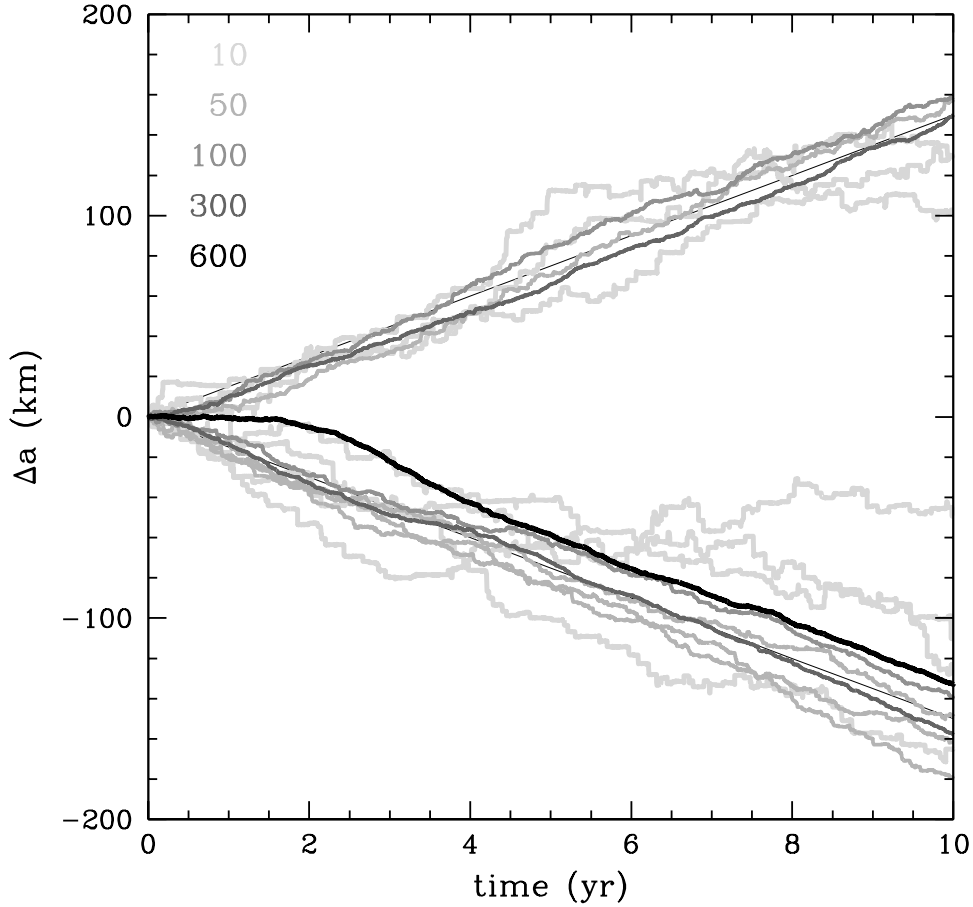


Fig. 8.— Fast migration of small moons in a ring of massive particles with  $\Sigma = 30 \text{ g/cm}^2$ . Each curve represents the change in orbital distance,  $\Delta a$ , of a moon with  $r_{\text{H}} = 14 \text{ km}$  that initially has a semimajor axis of 130,000 km. In each simulation the particles in the ring have identical mass, and are set to either 10, 50, 100, 300 and 600 times smaller than the mass of the moon. The darkest curve shows the case with the most extreme mass ratio (600:1); lighter shades have progressively less extreme mass ratios. The lightest curves, corresponding to runs where the particle masses are 10% of the moon mass, show stochastic behavior.

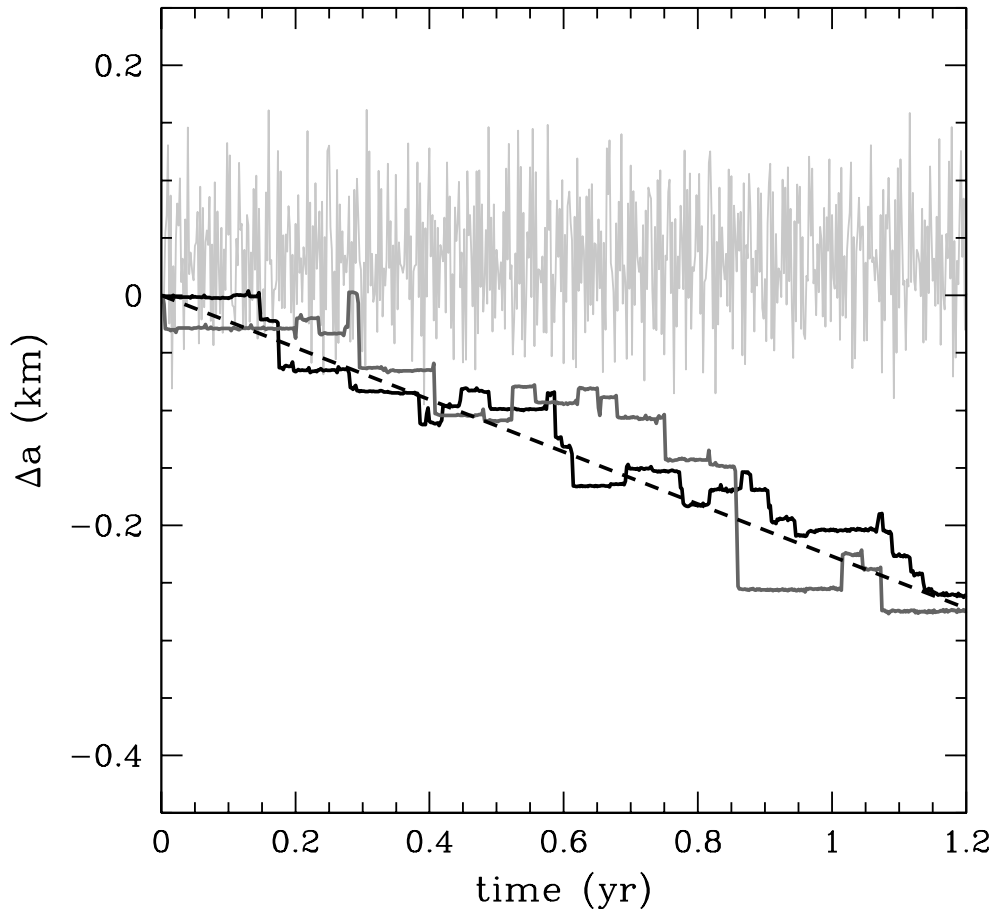


Fig. 9.— Fast migration of a small moonlet in the presence of Saturn’s massive moons. In these simulations a moonlet with  $r_H = 0.7$  km starts off at an orbital distance of 130,000 km in a ring with surface density  $\Sigma = 0.1$  g/cm<sup>3</sup>. The black curve corresponds to ring particles that are 1% of the moonlet mass, while the dark gray curve shows results for ring particles that are twice as massive. The corotation zone is initially clear, and no viscous diffusion can fill in the gap. Thus, fast migration ensues, and there is a subsequent change in orbital distance,  $\Delta a$  (solid black curve; the dashed line shows the theoretical prediction). Note that the true orbital distance (not shown) is given by the sum of  $\Delta a$  and the orbital fluctuations that result from orbital “jostling” of the moonlet by the distant moons. We estimate this jostling using a moonlet with identical starting conditions as the other simulations, but without any ring particles (light gray curve).

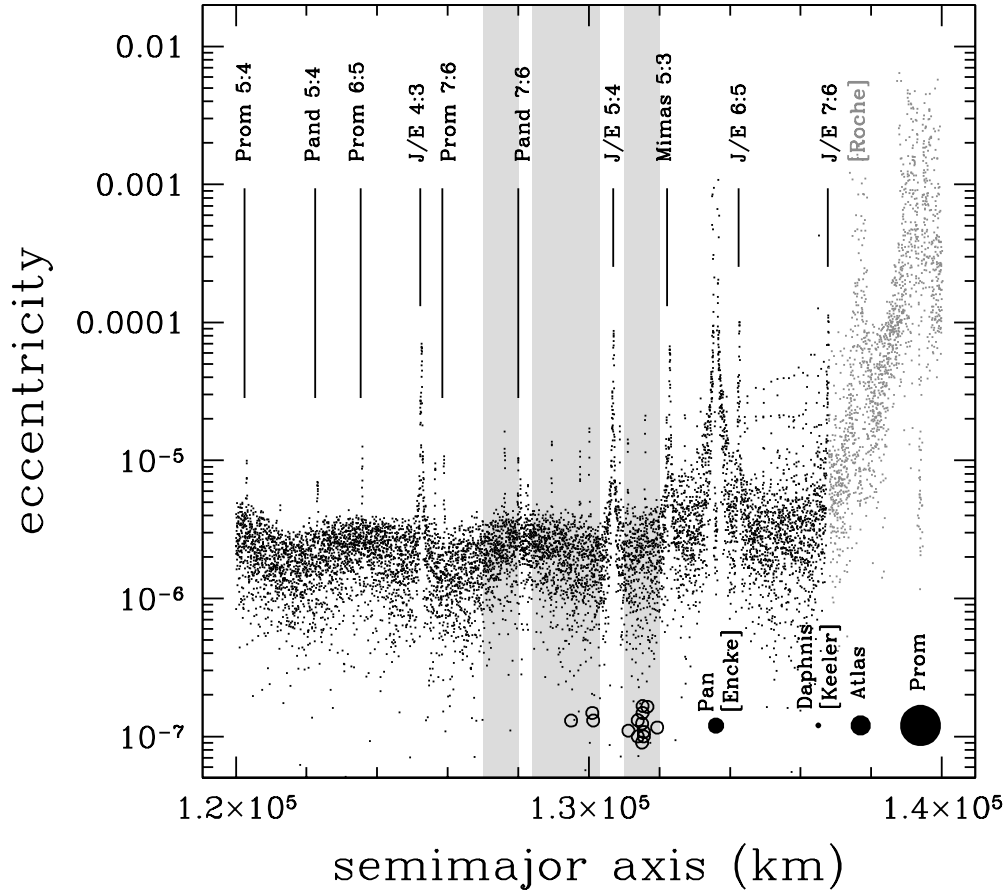


Fig. 10.— The eccentricity of simulated ring particles as a function of semimajor axis in the presence of massive moons. The simulation started from cold initial conditions and evolved tracer particles over a 4-year period. Some of the strongest resonances are labeled; off-resonance pumping of eccentricity is also apparent throughout the ring. The black circles designate moons; the size of each circle is suggestive of the relative mass. The open circles are a select sample of propeller moonlets from Tiscareno et al. (2008). None of these symbols are intended to quantify eccentricity, just the semimajor axis. The gray bands are the zones where propeller moonlets seem to reside exclusively. The figure also labels the location of the Encke and Keeler gaps, as well as the inner edge of the Roche Division (containing the light gray points).

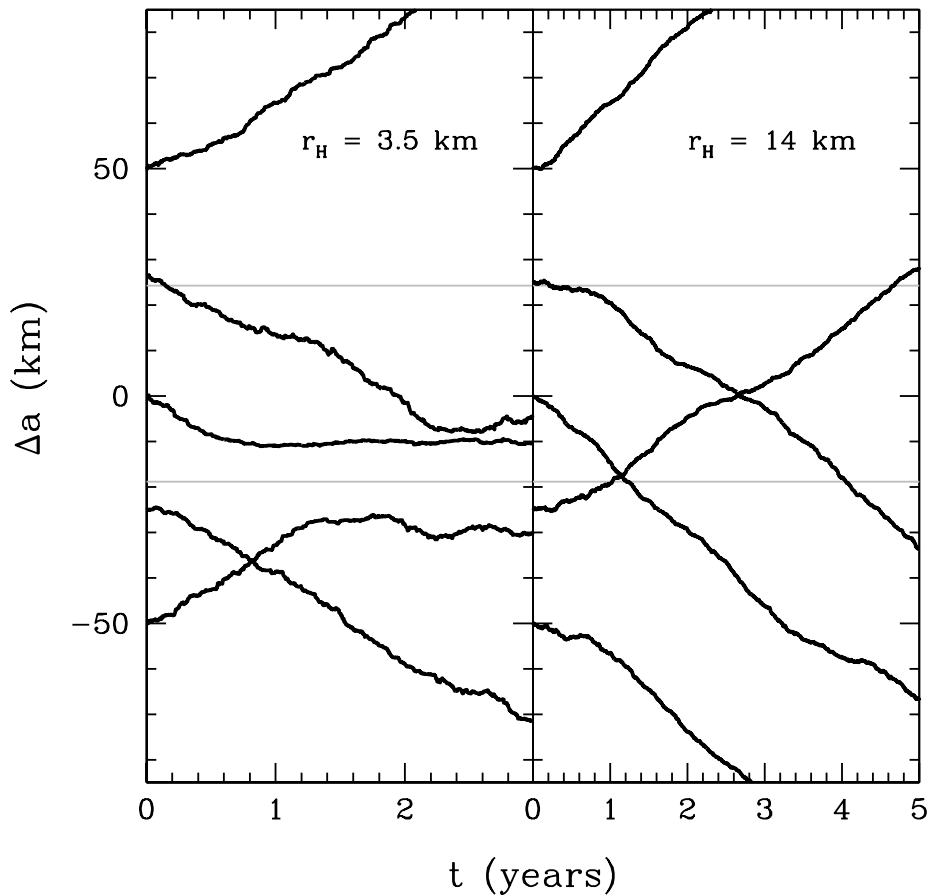


Fig. 11.— Fast migration in the presence of resonances from distant moons Janus and Epimetheus. The two panels show the output of simulations with isolated small moons on circular orbits at a position near the resonances. The black-colored traces show the radial position of each moon  $\Delta a = 0$  km relative to an orbital distance of  $a = 130,500$  km. For reference, the light grey lines give the location of the resonances from Janus and Epimetheus (upper and lower lines, respectively). The five runs in the left panel show fast migration of a smaller ( $r_H = 3.5$  km) moon; the runs in the right panel are for a larger moon ( $r_H = 14$  km). For each set of runs the initial conditions are identical, except that the moon and ring are radially offset by a differing amount. The results indicate that the smaller moons cannot cross the resonance; the larger ones can pass through.

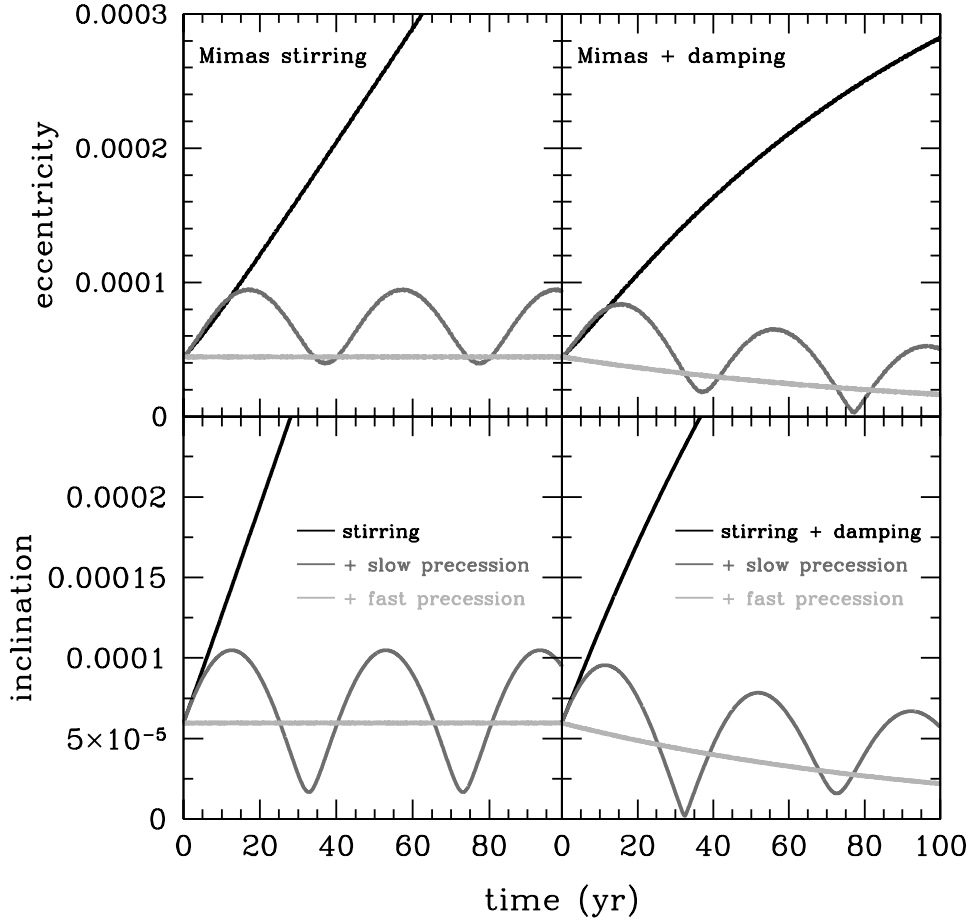


Fig. 12.— Stirring of a single massless ring particle by a distant moon (Mimas). The ring particle has initial orbital elements similar to Daphnis. Left panels: stirring by Mimas without collisional damping. Right panels: stirring by Mimas with collisional damping. In each panel, the black curves show the growth in  $e$  and  $i$  when Saturn and Mimas have a spherically symmetric gravitational potential. Stirring grows continuously. When Saturn’s oblateness is included in the calculations, the ring particle precesses rapidly. Stirring and precession yield a rough equilibrium in  $e$  and  $i$  as expected for a ring particle. When precession is slowed by a factor of 100, the variations in  $e$  and  $i$  become periodic due to the precession of the ring particle’s angular momentum vector precesses (dark gray curves).

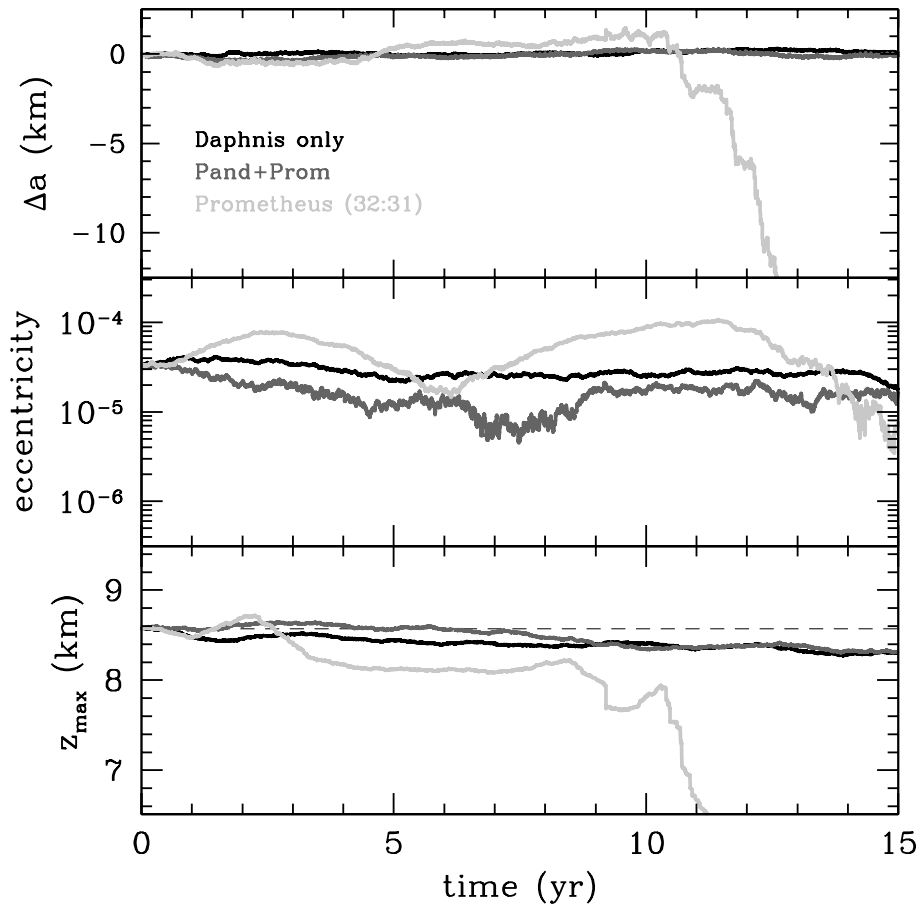


Fig. 13.— Simulations of Daphnis’ orbit: damping, stirring and resonances. The traces show changes in the semimajor axis (upper panel), eccentricity (middle panel) and maximum altitude above the ring plane (lower panel, the inclination is  $i \approx z_{\max}/a$ ) of a simulated moon with  $r_{\text{H}} = 2.6$  km at  $a = 136,505$  km. The initial eccentricity and inclination are similar to those of Daphnis (Jacobson et al. 2008). To help isolate physical effects, the oblateness of Saturn is not included in these simulations (see Fig. 12). The curves illustrate the evolution of (i) a small moon embedded in the Keeler gap (black curve), (ii) a small moon with its position adjusted to coincide with the 32:31 resonance of Prometheus (light gray curve), and (iii) a small moon, off-resonance but stirred by Prometheus and Pandora (dark gray curve). Without resonance or interactions with distant moons, Daphnis settles into the ring ( $\sim 10^2 - 10^3$  yr) and then begins fast migration. In a single resonance, Daphnis is scattered out of the Keeler gap and begins to migrate. Evolution within the Pandora 18:17 resonance is similar but on a longer timescale. Off resonances, the orbit is stable on timescales of at least  $10^4$  yr before Daphnis begins to settle into the ring.

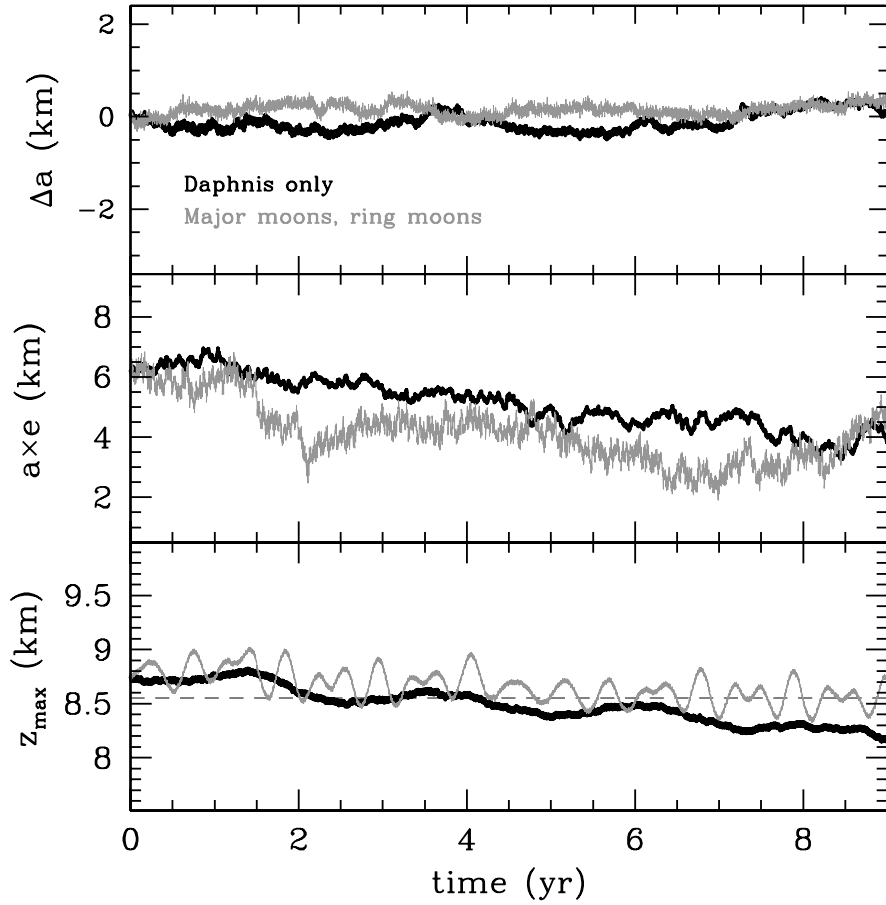


Fig. 14.— Simulated evolution of Daphnis’ orbit when stirred by Saturn’s moons. The moon orbits within a gap in surface density with a density contrast and width similar to the Keeler gap. As in Figure 13, the black curve shows changes in the moon’s orbital elements solely from interaction with the A-ring; over the course of 6000 orbital periods, Daphnis slowly settles in the ring and eventually begins to migrate rapidly. The light curve shows the evolution when Daphnis interacts with ring particles and all of the moons of Saturn. Using initial phase-space positions from JPL’s Horizons calculator (Giorgini et al. 1996), Saturn’s moons produce quasi-periodic fluctuations in the inclination, which prevent Daphnis from settling into the ring plane. Thus, interactions with distant moons plausibly prevent fast migration of Daphnis through the A ring.